An Oxford Nanopore-based Characterisation of Sputum Microbiota Dysbiosis in Patients with Tuberculosis: from baseline to 7 days after Antibiotic Treatment

John Osei Sekyere[#], Nontuthuko E. Maningi, Siphiwe Ruthy Matukane, Nontombi M. Mbelle, Petrus Bernard Fourie[#]

Department of Medical Microbiology, School of Medicine, Faculty of Health Sciences, University of Pretoria, South Africa.

#Address correspondence to Dr. John Osei Sekyere (jod14139@gmail.com) or Professor P Bernard Fourie (bernard.fourie@up.ac.za), Department of Medical Microbiology, University of Pretoria.

Running head: Antibiotic-based dysbiosis in TB patients

Tweet: "*Oxford Nanopore's MinION sequencer can be a useful tool for diagnosing tuberculosis and other polymicrobial infections, identifying resistance genes and mobile genetic elements, and monitoring treatment and its effect on the host's microbiome*"

Author summary

Tuberculosis (TB), one of the major killers of mankind, continually remains elusive as challenges with early diagnosis and treatment monitoring remain. Herein, we use a single portable sequencer from Oxford Nanopore, the minION, to diagnose TB and monitor its treatment with antibiotics using routine sputum samples. In addition, the presence of other pathogens, important commensals, antibiotic resistance genes, mobile genetic elements, and the effect of the antibiotic treatment on the sputum microbiota were determined from the same data. This makes the minION an important tool that can be used in clinical laboratories to obtain data that can inform live-saving decisions.

Abstract

Background. Diagnostics for tuberculosis (TB) and treatment monitoring remains a challenge, particularly in less-resourced laboratories. Further, the comprehensive sputum microbiota of TB patients during treatment are less described, particularly using long-read sequencers.

Methods. DNA from sputum samples collected from newly-diagnosed TB patients were sequenced with Oxford Nanopore's MinION. MG-RAST and R packages (Phyloseq, Microbiome) were used to determine the OTUs abundances, α/β diversities, functional components, OTUs networks and ordination plots. Statistical significance of the generated data was determined using GraphPad.

Results & conclusion. Antibiotics reduced the abundance and functional subsystems of each samples' microbiota from baseline until day 7, when persistent, tolerant, and resistant microbiota, including fungi, grew back again. Variations in microbiota abundance and diversity were patient-specific. Closer microbiome network relationships observed in baseline samples reduced until day 7, when it became closer again. Bacterial microbiota networks and spatial ordination relationships were closer than that of other kingdoms. Actinobacteria phylum and Mycobacterium were more affected by antibiotics than other phyla and genera. Parasites, viruses, and fungi were less affected by antibiotics than bacteria in a descending order. Resistance genes/mechanisms to important antibiotics, plasmids, transposons, insertion sequences, integrative conjugative elements were identified in few samples.

MinION can be adopted clinically to monitor treatment and consequent dysbiosis, and identify both known and unknown pathogens and resistance genes to inform tailored treatment choices, specifically in TB.

Keywords: *Mycobacterium tuberculosis; microbome; treatment monitoring; diagnostics; metagenomics.*

Introduction

Tuberculosis (TB), shall we ever overcome it? This question has been ringing through the annals of history over several millennia among diverse cultures and regions as the 'white plague' continues to devastate humanity and elude total eradication; a conundrum that still baffles clinicians, particularly with the current advancements in modern medicine [1–3]. Tuberculosis remains the deadliest infectious disease caused by a single aetiological agent, *Mycobacterium tuberculosis* (MTB), which is an acid-fast bacilli and intracellular bacterial pathogen [4–6]. In 2019, 1.4 million people died from TB alone, including 208,000 who had HIV [7]. Whereas TB is treatable and curable with first-line drugs such as isoniazid (INH) and rifampin (RFP), multidrug-resistant TB (MDR-TB), which was found in 206 030 people globally in 2019, requires more toxic, expensive, and scarce second-line chemotherapeutic agents that are taken for two years [5,7–9].

Until recently, the lung microbiome was believed to be sterile. However, the advent of non-culture-based techniques has shown the presence of a stable microbiota in the lung [6,10]. Furthermore, increasing evidence suggests that the intestinal microbiome modulates the lung microbiome through immune system regulation, development and inducement [11,12]. Several studies have shown that TB antibiotics, although taken orally, affect the upper and lower airways microbiome [4,6]. This interaction between the gut-lung microbiome is mediated through the immune system, and is being harnessed to enhance the treatment of asthma, cystic fibrosis, chronic obstructive pulmonary diseases (COPD) through the administration of probiotics and prebiotics that confers a microbiota than regulates inflammatory responses in the lungs [11–14]. Specifically, *Lactobacillus plantarum,* a gut commensal, has been shown to reverse TB progression and pathologies in the lungs [6]. A few studies have proposed the

presence and possible adoption of signature microbiota species that are indicative of the presence of TB and can be used for detection and treatment monitoring [15,16]. However, this is yet to be established and adopted as some studies also suggest otherwise [17].

The emergence and declining costs of whole-genome sequencing (WGS), with its varied applications in metagenomics [18,19], and meta-transcriptomics [20,21], are revolutionizing molecular biology research. Particularly, metagenomics promises a faster and more efficient detection of MTB infections and mixed infections, resistance profile, lineage of MTB strains, and epidemiological spread of TB outbreaks for efficient management and control of TB [1,18,22,23]. Thus, several propositions have been made to adopt WGS as a diagnostic tool for MTB in the clinical microbiology laboratory [1,18,22,23]. Of the 14 studies describing the microbiome of sputum samples from TB patients at the time of writing, none have so far used long-read sequencers such as Oxford Nanopore Technology's (ONT) MinION. All the reported studies either used Roche's 454/GS FLX-Titanium (pyrosequencing) or Illumina's Miseq/Hiseq to sequence the 16s rRNA [24–28]. Only one study has so far undertaken a shot-gun metagenomic analysis of bronchoalveolar lavage (BAL) samples of TB patients [29].

Hence, this study is the first to use a long-read sequencer to describe the sputum microbiota of TB patients. We show that the MinION can be adopted in clinical laboratories as a diagnostic tool to detect pathogens, monitor treatment outcomes and microbiota changes, and identify resistance genes/mutations and mobile genetic elements (MGEs).

Methods

Study design and sampling

This was a prospective study carried out at a TB clinic based at Stanza Bopape, Pretoria, South Africa, in 2019. Twenty-one patients were recruited between June and August 2019 for the study. Participants were persons newly confirmed to have pulmonary TB (using

GeneXpert), but who were not yet on treatment. Sputum samples were collected from each participant at four different timepoints: baseline (day 0), day 1, day 2, and day 7. Baseline samples were collected prior to the beginning of antibiotic therapy whilst days 1, 2, and 7 samples were collected one day, two days, and seven days after starting antibiotic treatment. As the patients were all newly diagnosed with TB, they were placed on fixed-dose combination (FDC) treatment involving first-line anti-TB drugs i.e., rifampicin, isoniazid, pyrazinamide, and ethambutol. Demographic data of the patients viz., age and sex, were also collected.

Sample treatment and sequencing

The collected sputum samples were transferred into the mycobacteriology laboratory (University of Pretoria) in wrapped sputum containers and stored at -4 ° Celsius. The samples were divided into two and one part was immediately dissolved in PrimeStore® Molecular Transport Medium (MTM) for long-term storage. Another part was immediately used for DNA extraction using the Ultra-Deep Microbiome Prep kit (Molzym GmbH & Co. KG, Bremen, Germany), which depletes host DNA and enriches microbial DNA. The extracted DNA was analysed using a NanoDrop spectrophotometer and gel electrophoresis to determine their quality, quantity, and length.

ONT's Rapid Barcoding Sequencing kit, SQK-RBK004, was used to prepare the DNA libraries for MinIon sequencing, following the recommended protocol. Briefly, the DNA (~400ng) of 12 samples were transferred into 12 DNA LoBind tube and adjusted with nuclease-free water up to 7.5µL; 2.5µL of Fragmentation Mix RB01-12 was added to make up to 10µL. The tubes were flicked gently to mix the contents and incubated at 30 °C (for1 min) and at 80 °C (for 1 min) to simultaneously fragment and tag the DNA with unique barcodes. The barcoded samples were then pooled into one 2 mL Eppendorf tubes and washed with AMPure XP beads and a magnetic rack to purify the barcoded DNA.

Subsequently, 1 µL of RAP was added to 10 µL of pooled barcoded DNA, incubated for 5 minutes, and mixed with 34 µL of sequencing buffer, 25.5 µL of loading beads, and 4.5 µL of nuclease-free water prior to loading into an already primed MinION FLO-MIN 106D R9/R10 flow cell. The sequencing was done for 12 hours per batch of 12 pooled barcoded samples. This was repeated for the other samples in batches of 12.

Bioinformatics and statistical analysis

The generated Fast5 sequences reads were de-barcoded into individual sample DNA and converted into FastQ files using the MinKNOW and EPI2ME applications provided by ONT. Sequence reads with coverage below 10X were deleted/removed. Initial taxonomy and resistance determinants in each sample were provided by EPI2ME. The FastQ files were assembled into FastA files using Canu 2.1 on Ubuntu 18.04LTS using default parameters. The assembled FastA files were uploaded to ResFinder 4.1(https://cge.cbs.dtu.dk/services/ResFinder/) /ResFinderFG 1.0 (https://cge.cbs.dtu.dk/services/ResFinderFG/), PlasmidFinder 2.1 (https://cge.cbs.dtu.dk/services/PlasmidFinder/), and Mobile Element Finder (https://cge.cbs.dtu.dk/services/MobileElementFinder/) databases to determine resistance mechanisms, plasmids, and mobile genetic elements respectively in the assembled reads.

The FastQ files were uploaded to MG-RAST [30], from where the distribution of functional categories for COGs, KOs, NOGs, and Subsystems, alpha diversities, rarefaction curves, taxonomies, sequence length histogram, and sequence GC contents per sample were obtained. Operational taxonomic units (OUT), metadata, and taxonomy tables were built from the MG-RAST data and used for downstream analyses in R using Phyloseq[31] and Microbiome (http://microbiome.github.com/microbiome) packages. The Chao1 and Shannon indices (alpha diversity), abundance of each taxonomy per sample, non-metric multidimensional scaling (NMDS), and ordination of the various taxa per sample were obtained using

Microbiome, Phyloseq[31], tidyr (https://tidyr.tidyverse.org/), dplyr (https://cran.r-project.org/web/packages/dplyr/vignettes/dplyr.html), and ggplot2 (https://ggplot2.tidyverse.org/) packages in R.

Beta diversities were manually calculated using the formula $\beta = (S1-c) + (S2-c)$, where β is the beta diversity, S1 is the total number of species in the first environment, S2 is the total number of species in the second environment, and c is the number of species that the two environments have in common. β diversities between samples from the same and different patients were thus calculated.

The significance of each taxa abundance across samples, of alpha and beta diversities per sample and between samples, and of archaea, bacterial phyla, viral, fungal, and parasitic taxa across samples were determined using Wilcoxon's signed rank test, one sample t test, and one-/two-way ANOVA. Descriptive statistics, row means, and variance were also determined using column statistics. All statistical analysis were carried out using GraphPad Prism 9.1.0 (221); p-values of <0.05 were defined as significant.

Ethical clearance

Ethical approval was provided by the Human Research Ethics Committee, Faculty of Health Sciences, University of Pretoria, South Africa. All protocols and consent forms were executed according to the agreed ethical approval terms and conditions. All clinical samples were obtained directly from patients, who agreed to our using their specimens for this research. The guidelines stated by the Declaration of Helsinki for involving human participants were followed in the study.

Data availability

This Whole Genome Shotgun project has been deposited at DDBJ/ENA/GenBank

under the Bioproject accession PRJNA673633 and Biosample accessions JAFMQ-JAFJNR000000000. The versions described in this paper is version JAFMQ-JAFJNR 010000000.

Results

Demographics and Sequencing reads

The study recruited 21 patients, aged between 23 and 55 years with an average age of 37.41 years and median age of 38 years. Six of the patients were females whilst 15 were males, with the females and males having a respective mean age of 30.60 and 40.25 years (Figure 1A; Dataset 1). Only 11 out of the 21 patients provided sputum samples within the time frame of the study. Complete sputum samples i.e., sputum samples collected at baseline, day 1, day 2, and day 7, were obtained from seven patients whilst three patients provided samples at baseline, day 1, and day 2. One patient provided only baseline and day 7 sputum samples (Fig. 1C). Only nine of the 11 sequenced reads qualified for inclusion in downstream analysis owing to their higher coverage (>10X) (Fig. 1D; Dataset 1). The sequence lengths ranged from 1529±738bp to 3396±1305bp whilst the mean GC contents ranged from 40±5% to 50±10% (Dataset 1).

Taxonomy, abundance, & diversities

A of total 40 phyla comprising 347 genera, belonging to Bacteria (n=258), Fungi (n= 50), Eukaryota (n=11), Animalia/Metazoa (n=8), Archaea (n=4), Plantae (n=3), Protista (n=2), and Chromista (n=1) were identified in the sputum samples (Dataset 2); variations in abundance for these kingdoms across samples were statistically significant. A core microbiota of 56 genera, which were present in at least 70% of all samples, was identified. The count of each genus for all the samples, categorised into abundances above 1000, between 100 and 1000, between 10 and 100, and below 10, showed that most genera fell

below a total abundance of 10 whilst a few fell above a total abundance of 1000. Streptococcus (p-value: 0.0078; <0.0001), Actinomyces (p-value: 0.1245; <0.0001), Mycobacterium (p-value: 0.1149; <0.0001), Granulicatella (p-value: 0.0432; <0.0001), Atopobium (p-value: 0.0078|<0.0001), Meyerozyma (p-value: 0.318;|<0.0313), Rothia (p-value: 0.1853|<0.0001), Catonella (p-value: 0.0884; <0.0001), Penicillium (p-value: 0.3076; <0.0078), Lactobacillus (p-value: 0.0272|<0.0001), Gemella (p-value: 0.0902; <0.0001), Veillonella (p-value: 0.2216; <0.0001), Candida (p-value: 0.0612; <0.0001), Pseudomonas (p-value: 0.0147; <0.0001), and Propionibacterium (p-value: 0.1174; <0.0001) were among the most dominant genera, with OTU abundance above 1000, in all samples (Figure S1).

The abundance of each OTU differed per sample, with baseline samples (D0) from patient 104 having the highest abundance. Notably, baseline samples from patients 104, 105, 107, 108, and 112 were higher than subsequent samples from days 1, 2, and 7 except in samples from patients 109 and 117 where baseline samples had lower genera abundance than samples from subsequent days (Fig. 2A; p-value: 0.005; <0.0001). Interestingly, samples from day 7 had higher OTU abundance than those from days 1 and 2, except in patients 107 (Fig. 2A). The absolute counts of the genera (diversity) per sample showed unique characteristics per patient. For instance, there were more diverse kinds of genera in baseline samples than samples from days 1 and 2 in patients 104 and 108, as well as than day 1 samples in patients 105, 107, 112, and 117. However, baseline samples were lower than samples from subsequent days in patient 109 (Fig. 2B). The highest genera count was in sample 108D0 (p-value: <0.0001).

Alpha and Beta diversities

The variation in alpha diversity (provided by MG-RAST) in samples from each patient was not consistent across patients; each patient had a unique variation in alpha diversity (p-value:

<0.0001). Specifically, there were variations in alpha diversities between samples from the same patient, but in patients 105, 108, 109, 111, 112, and 117, there was an increase in alpha diversities from either baseline or day 1 up to days 2 or 7 (Fig. 2C). The alpha-diversities were different from the absolute count of genera types per samples, which tended to follow a u-shaped pattern per patient (Figure 2B-C).

The Chao1 and Shannon alpha diversities (provided by Phyloseq) of each sample were not the same and also differed within patients (Figure S1). Whereas the alpha diversities between samples of the same patient were very close in the Chao1 index, they varied widely from each other in the Shannon index. Using the Chao1 index, there was a general reduction in alpha diversity of samples from baseline to days 1 and 2, except in patient 109. However, there was a rise in alpha diversity of the samples at day 7 after a drop in days 1 and 2. In patient 109, there was a rise in alpha diversity from baseline to day 1, after which the alpha diversity dropped from day 2 to day 7. Furthermore, in patient 117, the baseline diversity was higher than that on day 7. Patient 107 had a higher alpha diversity on day 2 than days 0 (baseline) and 1.

A similar pattern was observed in the Chao1 alpha diversity of bacterial genera in the samples. Generally, there was a drop in Chao1 alpha-diversity from baseline to days 1 and 2 samples whilst day 7 samples had higher alpha-diversity than baseline, day 1, and day 2 samples, suggesting a growing of drug-resistant/tolerant species during the 7^{th} day. The exception was observed in patient 117 where day 7 samples had lower alpha-diversity than baseline samples. Similarly, patient 107 had days 1 and 2 samples having higher alpha-diversities than baseline samples (Figure S2). However, the Chao1 and Shannon alpha-diversities of fungi, parasites/protozoa, and virus in the various samples showed relatively minor, little or no differences at all (Fig. S2.vii-ix).

A comparison of both Chao1 and Shannon alpha diversities of baseline and days 1, 2, and 7 samples from all patients are also shown in Fig. S2(iii-vi). For samples collected at any given timepoint (baseline, days 1, 2, and 7), there were variations between patients, highlighting personal microbiome diversity.

Figure 2B shows the β-diversities (differences in genera diversities) between different samples from the same patient (p-values: < 0.0001). The chart shows that there were variations in genera diversity between samples from different time points i.e., baseline (S1), day 1 (S2), day 2 (S3), and day 7 (S4), in all patients. Particularly, β-diversities of samples from patients 108 and 107 were very high, followed by that of patients 111, 109, 112, 117, 105, and 104. In patient 107, the β-diversity between days 0 and 1 (S1|S2) samples were very low compared to that of days 0 and 2 (S1|S3), days 0 and 7 (S1|S4), days 1 and 2 (S2|S3), and days 2 and 7 (S3|S4). However, in patient 108, inter-sample β-diversity was highest between days 0/baseline and 7 (S1|S4), days 0 and 1 (S1|S2), and days 0 and 2 (S1|S3). The inter-sample β-diversities variation per patient were not as relatively vast as that of patients 107 and 108.

The inter-patient samples β-diversities showed that the largest variations occurred in baseline samples from the different patients (blue bars in Fig. 2C). Specifically, β-diversity variations between samples of patient 108 and other patients were distinctly wide (p-value: <0.0001). Also notable were variations between days 2 (S3|S3) and 7 (S4|S4) samples' genera (Fig. 2C).

Kingdom-specific abundances

Analysis of the proportion of each kingdom in each collected sputum microbiota is presented in Figures 3A and S3. There were five main kingdoms viz. archaea, bacteria, virus, fungi, and parasites (protista), and minor kingdoms such as eukaryota, and animalia (metazoa). Bacteria

was the most dominant kingdom across all samples (p-value: <0.0086; < 0.0001) except in 107D2, 109D1, and 109D2, where fungi was most dominant (p-value: 0.2068; <0.0001). Parasites were also found in substantial proportions in 104D1, 105D2, 107D7, 108D1, 108D2, 109D1, 109D2, and 112D2 (p-value: <0.0047; <0.0001), but viruses (p-value: 0.0332; <0.0001) and archaea (p-value: 0.3277; >0.999) were very minor in abundance in all the samples (Fig. 3A & S3). A detailed breakdown of each phylum, class, order, family, and genus in each sample across all time points and in only baseline, day 1, 2, and 7 samples are shown in Figure S3.

Among Bacteria, the most common phyla were Firmicutes (p-value: 0.0069; <0.0001), Actinobacteria (p: 0.0348; <0.0001), Proteobacteria (p: 0.0066; <0.0001), and Bacteriodetes (p: 0.0037; <0.0001) (Fig. 4). In almost all the samples, the bacterial phylum Firmicutes was the most dominant, except in 105D2, 107D2, 108D1, and 112D2 where it was almost absent. Actinobacteria was the next dominant phylum, with Proteobacteria, Bacteroidetes and the other phyla occupying a relatively small portion of the microbiota. A reduction in bacterial phyla abundance was seen after the baseline until day 7, when a rise in abundance was observed again in all the samples (Fig. 3B). The most abundant genera were Streptococcus, followed by Mycobacteria (sea-blue bar), Actinomyces (orange bar), Pseudomonas (purple bar), and Rothia (mauve). Bacilli, Alphaproteobacteria, Actinobacteria, Epsilonproteobacteria, and Gammaproteobacteria were common bacterial classes whilst Clostridiales, Actinomycetales, Lactobacillales, Burkholderiales, and Micrococcales were the commonest bacterial orders that changed in abundance over the different time points (Fig. S4).

A u-shaped pattern was observed among bacterial genera in the various phyla (Fig. 4): the abundance of the genera reduced from baseline and rose gradually from day 2 to day 7. Genera diversity were not consistent from baseline to day 7; it was patient specific (Fig. 4).

290 This decline in abundance among the genera is more clearly observed in Figure 5; but
291 Mycobacterium continued declining after the baseline value (p: <0.0001). Detailed
292 breakdown of all bacterial taxonomic ranks and OTUs per sample collection time are
293 provided in Fig. S4.

294 Archaea was only present in 108D0 (baseline sample) and included only four genera:
295 Ferroglobus, Methanocaldococcus, Methanococcus, and Methanosaeta (Fig. 6A); none of the
296 abundance variations of these genera were statistically significant. Fifteen genera were
297 identified in all samples as parasites, with Codonosigidae (p: 0.0612; <0.0001) and
298 Schistosoma (p: 0.0014; <0.0001) being the most abundant and common. Notably, the
299 variations in abundance in parasitic genera were not consistent between baseline and days 1,
300 2, and 7; most of these genera had non-significant variations in abundance (Dataset 3). In
301 patient 104, there was a reduction in abundance in parasitic genera from baseline to day 7, but
302 this was not the case in other patients. In 105, there was a rise in parasitic genera on day 2
303 and a fall on day 7. In 107, there was a sharp fall in parasitic genera abundance on day 1, a
304 gradual rise on day 2, and a sharp rise on day 7, which was higher than that of the baseline.
305 Similarly, a sharp rise in parasitic genera was observed on days 1 and 7 in 109. However, a
306 gradual rise in parasitic genera was observed in 108 up to day 2, when it dropped
307 significantly on day 7 (Figure 6B).

308 Under parasites were kingdoms such as Animalia, Chromista, Eukaryota, Metazoa, and
309 Protista, which varied across the different time points after commencement of antimicrobial
310 chemotherapy. Further breakdown of the various taxonomic ranks under these kingdoms per
311 sample is shown in Figure S5.

312 Unlike parasites, fungi were not found in all samples although there were 51 fungal genera,
313 making them the second most common kingdom after bacteria. Specifically, fungi were

absent from patient 104, and in samples 105D0, 107D0, 107D1,108D1, 108D2, 109D7 and 117D7. Saccharomyces (p: 0.0821; 0.0078) was a common fungi genus in the samples, particularly in 105D2, 105D7 and 106D7. Other common fungi genera were Penicillium (p: 0.3076; 0.0078), Meyerozyma (p: 0.318; 0.0313), and Debaryomyces (p: 0.163; 0.0625). Variations in abundance and diversity of fungal genera were observed across different time points in some samples, but none of the genera had significant variations in abundance across the samples (Dataset 3). Particularly, there was a sharp rise in Saccharomyces in 105D2 and 105D7, albeit there was none in the baseline, suggesting that it increased in the microbiota after antibiotics were introduced. There was a drop in abundance of Penicillium from 107D2 to 107D7 whilst several fungal genera such as Meyerozyma and Saccharomyces emerged, increasing the diversity. Changes in fungal abundance and diversity were also observed in patients 108, 109, and 111 (Fig. 6C). Detailed breakdown of fungal genera per sample according to taxonomic rank is shown in Figure S6.

Viruses from Siphoviridae were the commonest and most abundant in all samples, particularly baseline samples from patients 104, 107, 108, 112, and 117 as well as day 7 samples from patients 105, 106, 107, 108, 109, and 117. Notably, viruses, including Siphoviridae, were almost absent in days 1 and 2 samples, except in 105D2, 107D2, and 111D1. Myoviridae, Podoviridae, and T4-like viruses were also present in mainly baseline samples and to a lesser extent, day 7 samples, from patients 105, 106, 107, 108, 112, and 117; 107D2 was the only day 2 sample with these viruses (Fig. 6D). None of the viral OTUs had significant variations in abundance across the samples (Dataset 3). Detailed viral OTUs per taxonomic rank in each sample is detailed in Figure S7.

Functional subsystems components

A functional subsystem component analyses (generated by MG-RAST) showed the proportional changes in key cellular processes and components in each sputum sample from

baseline through days 1, 2, to 7. Instructively, the functional component of each sample was strongly/significantly associated with its abundance in that sample (Dataset 3). The major functional subsystems in all the microbiota samples were clustering-based subsystems, carbohydrates, protein metabolism, DNA and RNA metabolism, cofactors, vitamins, prosthetic groups & pigments, and cell wall and capsules. Baseline and to some extent, day 7, samples had the most abundant and diverse functional subsystems compared to those of days 1 and days 2. The functional components of the sputum microbiota decreased from baseline to day 2 and increased gradually on day 7. An exception was observed in samples 109 and 117, in which day 7 samples had higher abundance and diversity of functional components than the baseline samples (Fig. 7).

Network and ordination analysis

The spatial relationship and networking between the microbiota in the sputum samples collected at different time points showed a reduction in the microbial networks from baseline to day 7, with a thickening of the networks on day 7. The closer connection seen in the networks shows the close interactions between the microbiota. Compared to bacteria, network analyses for parasites were relatively less busy and interconnected. The changing diversity of the phyla or classes (OTUs) in the collected samples at different time points is also seen in the widening network distances and reducing interconnections between the various classes (OTUs) (Figures 8, S9 and S10).

In the nonmetric multidimensional scaling (NMDR) ordination plots, a closer spatial relationship existed between bacteria than fungi, virus, and parasite OTUs. Gammaproteobacteria, Bacilli, Erysipelotrichia, Clostridia, and Actinomycetes, filled distinct spaces distant from other classes that clustered together. The greatest change in ordination was seen in bacterial classes. The day 1 ordination was closer to each other than the baseline

plots. Virtually no change was observed between the classes of other kingdoms in day 1 and baseline (Fig. S10).

Resistance genes and mobile genetic elements

Resistance determinants to tetracyclines (*tet*), aminoglycosides (*aph, aac(2'), aac(3')*), macrolides (*erm, mef, msr*), quinolones (*qnrD,* unknown *gyrAB* mutations), isoniazid (*kat*G: N138T, K143T, Y155S), capreomycin (*tly*A: A67E), para-aminosalicylic acid (*ribD*: G8R), rifampicin (*rpoC*: F6V, F7A, L10H, W23R, S24*), ethionamide (ethR: R19?, D96G, R164?, T165?), pyrazinamide (*pncA* mutations), and ethambutol (*embR* mutations) were found in only eight sputum samples. Mobile genetic elements such as plasmids (ColRNAI, repUS38, repUS43, rep5e, repUS34), transposons (Tn253), integrative conjugative element (ICE) and insertion sequences (IS30, ISL, IS3, IS4, IS1182) were also found either alone or in association with antibiotic resistance determinants in 13 samples (Dataset 2).

Discussion

In this work, we show how ONT's MinION can be used to monitor the treatment outcome of TB, detect MTB and other associated bacterial, fungal, parasitic, and viral pathogens, identify antimicrobial resistance determinants and mobile genetic elements, and monitor microbiota changes (dysbiosis) during antimicrobial chemotherapy using sputum. Hence, the importance of using this portable technology in clinical settings to diagnose infections, inform antimicrobial treatment choices, monitor the effects of antimicrobials on the gut, oral, upper airways and lungs microbiota, despite its inherent challenges, cannot be gainsaid.

Using sputum samples from patients freshly diagnosed with tuberculosis, it was observed that the microbiota of the sputum samples collected prior to the initiation of antibiotic therapy (baseline samples) comprised of more diverse and abundant microbial genera (OTUs) than that observed in days 1, 2, and 7 (Fig. 2-6). Albeit there were a few exceptions to this pattern,

the higher abundance and diversity of microbiota in the sputum of untreated patients testify to the effect of antitubercular drugs on the sputum microbiota. Thus, although the antibiotics are taken orally, they become bioavailable in the sputum through the blood.

It is interesting to note that the microbial abundance and diversity began to increase on day 7 after onset of treatment, suggesting the regrowth of persistent, tolerant or resistant microbiota after day 7 of treatment. However, this was not observed with Mycobacterium, which continued declining even after day 7. This is expected because the antibiotics given to the patients, i.e. isoniazid, rifampicin, pyrazinamide, and ethambutol, are narrow-spectrum antibiotics targeting Mycobacterium. Notwithstanding the narrow spectrum nature of these antibiotics, they did affect the abundance and diversity of the microbiota, including bacteria, fungi, parasites, and viruses, although their effect on non-bacterial microbiota were relatively limited (Figure 2-5). Recently, Kateete et al. (2021) observed a significant mean reduction in the microbiotia biomass in the sputum of TB patients 2 months after onset of treatment. Further, Sala et al. (2020) found non-significant changes in microbiota diversity in sputum of TB patients up to 7 months. As the authors did not collect and analyse samples at day 7, a comparative analysis cannot be made [17,32].

The change in microbial abundance and diversity after antibiotic treatment reflected in the functional components subsystems dynamics, ordination plots and network analyses (Fig. 7-8; S8-S10). Particularly, the abundance of each functional subsystem in samples collected from the same patient from baseline to day 7 also dropped on days 1 and 2, and rose on day 7 whilst the network relationship between the microbiota reduced from baseline samples until they increased on day 7. This is expected, as the biocidal action of the antibiotics on the microbiota will definitely reduce the number of microbes and their functions in the upper air ways (Fig. 7). Hence, any beneficial effect of the microbial activity in the upper airways, including the production of metabolites important to the host, will be negatively affected.

Further, the regrowth of the microbiota and the increase in their metabolic functions from day 7 suggests the evolution and emergence of tolerance, persistence, and resistance, which numbs the effects of the antibiotics on these microbes. Further, the reducing microbial abundance also reduced the spatial interrelationship between the microbes until day 7, when they grew back and strengthened the networks between them again (Fig. S9-S10). This shows the short-term effect of antibiotics in generating resistance and demonstrates why it is inadvisable to use antibiotics beyond a week for normal infections.

The functional components and subsystems of the microbiota (Fig. 7) gives a comprehensive overview of the cellular activities (metabolic pathways), components, and metabolites produced by the microbiota. Notably, most of the samples were dominated by clustering-based subsystems (contain functions such as proteosomes, ribosomes and recombination-related clusters), carbohydrates, protein metabolism, RNA & DNA metabolism, amino acids and derivates, co-factors, vitamins, prosthetic groups and pigments, cell wall and capsule, fatty acids, lipids and isoprenoids, nucleotides and nucleosides, membrane transport, virulence, disease and defence, phages, prophages, transposable elements and plasmids, and regulation and signaling. Obviously, all these subsystems are necessary for the normal functional activities of the cell, except prophages, transposable elements and plasmids, and virulence, disease, and defence. Hence, most of the metabolic activities of the sputum microbiota were focused on maintaining cellular life.

Other studies characterising microbial communities in termite mound soils[33], grassland soils [34], and water reservoirs [35], also found a similar composition and abundance in the microbial communities, confirming that these processes are basic to cellular life irrespective of the ecological niche. It's interesting that dormancy and sporulation structures were reduced to the basic minimum on day 1 and rose on day 7, limiting the possibility that antibiotic exposure could have increased dormancy and sporulation among the microbiota. Sharma et al. (2017)

observed a downregulation of MTB genes involved in ATP synthesis, aerobic respiration, translational and section machinery, etc. whilst there was no differential expression in dormancy genes (*dos*RS), suggestive of a low energy, low metabolism, and low replication state in the sputum [36].

The α-diversities show that each patient had a unique microbiome with different microbiota composition and metabolic/functional subsystems that reacted quite similarly to antibiotics (Fig. 2C & 7). The changing within-host α-diversities show that antibiotics affect the microbial diversity (Fig. 2C). This is further corroborated by the inter-sample diversity within and between hosts (Fig. 2D). In particular, samples from patients 107 and 108 were very diverse from each other as well as from other samples. In all patients, changes between baseline and days 1 and 2 samples were substantial (Fig. 2D-E), representing the significant shift in diversity from baseline to days 1 and 2 after antibiotic treatment. A change in α-diversity was also noticed recently in MTB+ patients BAL microbiome [29]. Notably, some authors have observed little or no differences in sputum microbiome diversity between TB and non-TB patients from non-Africa settings [17,28]. Specifically, the sampling points, 16s rRNA and pyrosequencing used were different from that used herein. Hu et al. (2020) argue that 16s rRNA-based analysis of TB-microbiome provides lower resolution than whole-genome shot-gun metagenomics [29].

The sputum microbiota was dominated by bacteria, followed by fungi and a few parasites, viruses, and archaea. Firmicutes was the most abundant phylum among bacteria, followed by Actinobacteria and Proteobacteria. Similar microbiota compositions, albeit with little shifts in relative abundance, have been reported in other studies using 16s rRNA or shot-gun metagenomics on either sputum or BAL from TB patients [15–17,25–29,32,36–41]. Compared to the dysbiosis in all the microbiota (Fig. 2), the bacterial dysbiosis was most pronounced, with a substantial drop in abundance being observed on day 1 (Fig. 3). Streptococcus was the most

462 dominant genera in Firmicutes (Fig. 4)[28,32,39,40], whose abundance was also affected by the
463 antibiotic-mediated dysbiosis. In patient 105, Leuconostoc replaced Streptococcus as the
464 most dominant genera on days 1 and 2. In patient 104, Gemella, Clostridium,
465 Staphylococcus, Solobacterium, and Erysipelotrichaceae increased on day 1. Coprobacillus
466 increased in abundance in 108D1 and 108D2. Similar patterns were observed in almost all
467 samples, in which different genera emerged after a reduction in Streptococcus abundance
468 (Fig. 4A).

469 Unlike Firmicutes, no single genera dominated the phylum Proteobacteria, albeit
470 Pseudomonas was common in many samples (Fig. 4B) [16,29,39]. Specifically, baseline and day
471 7 samples were dominated by Pseudomonas, suggesting that Pseudomonas was affected by
472 the antibiotics, but grew back on day 7. Neisseria was very common in 104D0, but virtually
473 absent in subsequent days, which also suggest that it was affected by the antibiotics. There
474 was a notable rise in Achromobacter in 107D1, but it diminished again on 107D1-D7, where
475 it was replaced by Pseudmonas, Klebsiella, and Proteus. These dynamics only confirm that
476 susceptible genera were giving way to more tolerant, persistent, and resistant Proteobacterial
477 genera.

478 The phylum Actinobacteria was dominated by Mycobacterium, Atopobium, Actinomyces,
479 and Rothia, which has been found by Hong et al. (2018) to be always co-occurring with MTB
480 [15,16,29]. Unlike the phyla Firmicutes and Proteobacteria, the effect of the antibiotics on
481 Actinobacteria were more drastic. This is not surprising as Mycobacterium, which these
482 antibiotics mainly target, are found within this phylum (Fig. 4C). Moreover, compared to the
483 other phyla, the members of this phyla did not grow back on day 7; except 108D7. Thus, anti-
484 mycobacterial drugs were more effective against Actinobacteria than other phyla (Fig. 4).

Other bacterial phyla, including Aquificae, Bacteroidetes, Fusobacteria, Fibrobacteres, Chlorflexi, Cyanobacteria, Deinococcus-Thermus, Nitrospirae, Planctomycetes, Spirochaetes, Synergistetes, Tenericutes, and Verrucomicrobia were also found in the sputum microbiota[28,29,32,39]. Among these phyla, the commonest were Bacteroidetes (Bacteroides, Prevotella), Fusobacteria (Fusobacterium), Synergistetes, Spirochaetes (Treponema), Tenericutes (Candidatus phytoplasmsa), and Cyanothece (Cyanobacteria). These phyla were also affected by the antibiotics as their abundance and diversity dropped after baseline and rose on day 7. However, in patients 107 and 108, these phyla increased in abundance on days 1 and/or 2 than on day 7, with shifts in genera diversity/composition, suggesting the proliferation of resistant and/or persistent genera (Fig. 5).

An example of the MinION's ability to identify other potentially pathogenic genera is shown in Fig. 5 where genera such as Streptococcus (Fig. 5A), Mycobacterium (Fig. 5B), Clostridium, Schistosoma, Neisseria, Enterococcus, and Staphylococcus (Fig. 5E-F) were detected. This makes the MinION a potential diagnostic tool that can be used to detect not only *Mycobacterium tuberculosis* using sputum samples, but also other pathogens that inhabit the oral and pharyngeal cavities. Particularly in polymicrobial or secondary infections, this tool can help clinicians identify all pathogens in the patient's sample, informing appropriate antimicrobial choices. Further, it can be used to monitor treatment in patients by measuring the abundance of any pathogen over time. In this case, the efficacy of the antimicrobial agents could be seen in the declining abundance of the various genera, including Mycobacterium. When there is a regrowth of the targeted pathogen, in this case *M. tuberculosis*, the clinician can see it and change the antibiotics used. Finally, the shifts in the microbiota can also inform the clinician of the extent of antibiotics-mediated dysbiosis and its potential effects on the immunity and emergence of other non-susceptible and diarrhoeagenic

pathogens such as *Clostridium difficile,* Shigella, *Escherichia coli* etc. that can complicate or prolong healing [6,24].

There was a more significant effect of the antibiotics on parasites than on fungi and viruses (Fig. 6; Dataset 3). Interestingly, in patients 105 and 107, the identified fungi genera only grew after days 2 and 7, suggesting their proliferation after the decline in the bacterial population. Similarly, in patient 108, the fungi found in the baseline samples all diminished on days 1 and 2, only to be replaced with different fungi on day 7 whilst patients 109 and 112 had different genera replacing those found in their baseline samples. These observations show that the antibiotics provided advantage to other fungal genera to outgrow others. Codonosigidae and Cryptosporidium seemed tolerant and more resistant to the antibiotics than the other parasites as they were able to grow on days 1 to 7 with little or no reductions and substantial increments (Fig. 6; Dataset 3). Fungi belonging to Ascomycota and Basidiomycota (Fig. S6) were detected in both sputum and oropharyngeal TB samples with similar community structures [26]; however the effect of antibiotics on these phyla were not described.

Although antibiotics have no effect on viruses, reductions were seen in the abundance of Siphoviridae, Myoviridae, and Podoviridae. This could be an indirect effect through antibiotics action on bacteria, fungi, and parasites, which could be serving as cellular hosts to the viruses, which cannot exist outside of living cells. Therefore, the reducing abundance of bacteria, fungi, and parasites could be ridding the viruses of important hosts in which they can multiply, affecting their abundance as well. This demonstrates that antibiotics-mediated microbiota dysbiosis can also affect the virome population. Hence, as the bacteria, fungi, and parasites populations increased on day 7, that of the viruses also increased in tandem (Fig. 6; Dataset 3).

The network analysis and ordination plots show that there is a closer interaction between bacterial genera, including Mycobacterium, than between non-bacterial ones. This closer association was affected by antibiotics, evincing the effect of dysbiosis on the ecology of the microbiome [4,6,24]. The effect of such an interaction, or its lack thereof, on the pathogenesis of *M. tuberculosis* is yet to be established, although dysbiosis has been associated with increased TB pathologies. Obviously, the beneficial effects of the microbiota and their interactions on the immune system, including their production of metabolites, indirectly affects the pathogenesis of *M. tuberculosis* [4,6,24].

Analysis of the microbiota across the samples shows the presence of external genera that are not commonly found in or part of the core oral microbiome. Examples include Stenotrophomonas, Cupriavidus, Sphingomonas, Brevibacillus, and the anaerobe, Lautropia [24,27]. Except for Lautropia and Brevibaccilus, the others were found in day 1 or 7 samples. Whereas Naidoo et al. (2021) found an enrichment of Lautropia in sputa microbiota of treatment-naïve TB patients, this was not the case in our data [24]. However, these observations shows the invasion of external microbiota in the upper airway microbiome due to TB or antibiotics therapy.

The antibiotic resistance mechanisms and MGEs of the microbiota in the sputum samples were determined and found to be relatively few. It is noteworthy that all the recruited patients were newly diagnosed with TB and were not found to have rifampicin or multidrug resistance by GeneXpert and the line probe [5,6,8,9,42]. However, an analysis of the microbiota identified resistance-mediating mutations in genes that confer resistance to TB drugs such as aminoglycosides, quinolones, isoniazid, capreomycin, rifampicin, ethambutol, ethionamide, and pyrazinamide as well as to non-TB antibiotics in a few of the samples; particularly, 108D0 [5,8,9]. The absence of these mutations in subsequent samples could suggest that these mutations were not enough to withstand the effect of all four antibiotics combined. Moreover,

this evidence shows that the MinION can not only detect the presence of Mycobacterium but also its resistance profiles, and possibly lineage, in sputum samples, particularly when sequenced at a higher coverage. The resistance mechanisms of the other microbiota and their MGEs can also be determined to inform important clinical decisions.

Finally, the data suggests that age and sex had little to do with the outcome of the findings as same or similar patterns were observed in samples from different ages and sexes; findings by Wu et al. (2013) also concur [39]. Larger cohorts may be necessary in future studies to confirm the absence of any effect of age and/or sex on the sputum microbiota and its response to anti-tubercular therapy.

Conclusion

ONT's MinION sequencer is a portable device that can be used to detect Mycobacterium in sputum samples of patients newly diagnosed with TB, monitor their response to treatment, detect the presence of other pathogens (polymicrobial infections) in the sputum samples, identify resistance genes and MGEs, and monitor the effect of administered antibiotics on the sputum microbiota. With the introduction of advanced flow cells and kits that can multiplex at most 96 samples (https://store.nanoporetech.com/us/pcr-barcoding-expansion-1-96.html), it is even cheaper and faster to detect the presence of *M. tuberculosis* and other pathogens, their resistance and virulence mechanisms as well as their MGEs in clinical samples within 6-48 hours. The presence of other pathogens that may not be targeted by routine microbiological assays, can be easily detected by the MinION, helping clinicians treat polymicrobial and idiopathic infections. The sequence lengths produced by the MinION, which ranged from 1500-4000bp, coupled with higher coverage, can enhance its sensitivity and specificity for detecting all commensals and pathogens as well as their clones/lineages.

The comprehensive data provided by this new technology makes it ideal for clinical microbiology laboratories to detect all pathogens with little laboratory accoutrements. We show that the oral administration of anti-tubercular chemotherapy affects the sputum microbiota by reducing their abundance and shifting their diversity from onset of treatment (day 1) until day 7, when persistent, tolerant, and resistant microbiota, including fungi, begins to grow back to replenish the microbiome. Hence, antibiotics usage after one week should be done with caution as it can result in drug-resistant infections.

Funding sources: This study was funded by (1) South African National Research Foundation Grant number UID 127338; (2) CRDFGlobal Grant number DAA9-20-66880-1.

Acknowledgement: We are grateful to the following persons for their help in this work. (1) Patient screening: Sr Mkhondo, Stanza Bopape Community Health Centre TB Clinic, Pretoria; (2) Field work and specimen collections: Ms Phindile Ntuli, Ms Sharon Olifant; (3) Donation of PrimeStore Molecular Transport Medium: Longhorn Vaccines and Diagnostics, San Antonio, TX (only if the product is mentioned in the manuscript).

We especially dedicate this work to the memory of Professor Nontombi Marylucy Mbelle Ph.D., who passed away in January 2021, prior to the completion and submission of this work.

Transparency declaration: The authors declare no conflict of interest and the funders had no influence or decision whatsoever in the decision to write-up and publish this work.

Author contributions: JOS designed and carried out all the laboratory (experimental), sequencing, bioinformatics, and statistical aspects of this work. He also wrote the article and formatted for publication. **NEM** and **SRM** assisted with the experimental sections of this work. **NMM** assisted with funding and sequencing reagents for this work. **PBF** supervised

this work and provided funding for it. All authors reviewed this work prior to submission for publication.

References

1. Kay, G. L. *et al*. Eighteenth-century genomes show that mixed infections were common at time of peak tuberculosis in Europe. *Nat. Commun.* **6**, 1–9 (2015).
2. Donoghue, H. D. Insights into ancient leprosy and tuberculosis using metagenomics. *Trends Microbiol.* **21**, 448–450 (2013).
3. Cambier, C. J., Falkow, S. & Ramakrishnan, L. Host Evasion and Exploitation Schemes of Mycobacterium tuberculosis. *Cell* **159**, 1497–1509 (2014).
4. Naidoo, C. C. *et al.* The microbiome and tuberculosis: state of the art, potential applications, and defining the clinical research agenda. *The Lancet Respiratory Medicine* **7**, 892–906 (2019).
5. Osei Sekyere, J., Reta, M. A., Maningi, N. E. & Fourie, P. B. Antibiotic resistance of Mycobacterium tuberculosis complex in Africa: A systematic review of current reports of molecular epidemiology, mechanisms and diagnostics. *Journal of Infection* **79**, 550–571 (2019).
6. Osei Sekyere, J., Maningi, N. E. & Fourie, P. B. Mycobacterium tuberculosis , antimicrobials, immunity, and lung–gut microbiota crosstalk: current updates and emerging advances. *Ann. N. Y. Acad. Sci.* **1467**, 21–47 (2020).
7. WHO. *Global Tuberculosis Report 2020*. *Who* (2020). doi:WHO/HTM/TB/2017.23
8. Maningi, N. E. *et al.* Multi- and Extensively Drug Resistant Mycobacterium tuberculosis in South Africa: a Molecular Analysis of Historical Isolates. *J. Clin. Microbiol.* **56**, JCM.01214-17 (2018).
9. osei Sekyere, J., Maphalala, nontobeko, Malinga, L. A., Mbelle, nontombi M. & Maningi, nontuthuko E. A Comparative Evaluation of the New Genexpert MTB/RIF Ultra and other Rapid Diagnostic Assays for Detecting Tuberculosis in Pulmonary and Extra Pulmonary Specimens. *Sci. Rep.* **9**, (2019).
10. Dickson, R. P. & Huffnagle, G. B. The Lung Microbiome: New Principles for Respiratory Bacteriology in Health and Disease. *PLoS Pathog.* **11**, 1–5 (2015).
11. Shukla, S. D., Budden, K. F., Neal, R. & Hansbro, P. M. Microbiome effects on immunity, health and disease in the lung. *Clin. Transl. Immunol.* **6**, e133 (2017).
12. O'Dwyer, D. N., Dickson, R. P. & Moore, B. B. The Lung Microbiome, Immunity and the Pathogenesis of Chronic Lung Disease. *J Immunol* **196**, 87–92 (2016).
13. Hauptmann, M. & Schaible, U. E. Linking microbiota and respiratory disease. *FEBS Lett.* **590**, 3721–3738 (2016).
14. Evsyutina, Y., Komkova, I., Zolnikova, O., Tkachenko, P. & Ivashkin, V. Lung microbiome in healthy and diseased individuals. *World J. Respirol.* **7**, 39–47 (2017).
15. Hong, B. young, Paulson, J. N., Stine, O. C., Weinstock, G. M. & Cervantes, J. L. Meta-analysis of the lung microbiota in pulmonary tuberculosis. *Tuberculosis* **109**, 102–108 (2018).
16. Hu, Y. *et al.* Distinct lung microbial community states in patients with pulmonary tuberculosis. *Sci. China. Life Sci.* **63**, 1522–1533 (2020).
17. Sala, C. *et al.* Multicenter analysis of sputum microbiota in tuberculosis patients. *PLoS One* **15**, e0240250 (2020).
18. Doughty, E. L., Sergeant, M. J., Adetifa, I., Antonio, M. & Pallen, M. J. Culture-independent detection and characterisation of Mycobacterium tuberculosis and M . africanum in sputum samples using shotgun metagenomics on a benchtop sequencer. *PeerJ* **2**, 1–18 (2014).
19. Zhang, Y., Lun, C. Y. & Tsui, S. K. W. Metagenomics: A newway to illustrate the crosstalk between infectious diseases and host microbiome. *International Journal of Molecular Sciences* **16**, 26263–26279 (2015).
20. Martinez, X. *et al.* MetaTrans: An open-source pipeline for metatranscriptomics. *Sci. Rep.* **6**, 1–12 (2016).
21. Bashiardes, S., Zilberman-schapira, G. & Elinav, E. Use of Metatranscriptomics in Microbiome Research. *Bioinform. Biol. Insights* **10**, 19–25 (2016).
22. Lee, R. S. & Behr, M. A. The implications of whole-genome sequencing in the control of tuberculosis. *Ther. Adv.*

Infect. Dis. **3**, 47–62 (2016).

23. Witney, A. A. *et al.* Clinical use of whole genome sequencing for Mycobacterium tuberculosis. *BMC Med.* **14**, 46 (2016).

24. Naidoo, C. C. *et al.* Anaerobe-enriched gut microbiota predicts pro-inflammatory responses in pulmonary tuberculosis. *EBioMedicine* **67**, 103374 (2021).

25. Eshetie, S. & Van Soolingen, D. The respiratory microbiota: New insights into pulmonary tuberculosis. *BMC Infect. Dis.* **19**, 1–7 (2019).

26. Botero, L. E. *et al.* Respiratory tract clinical sample selection for microbiota analysis in patients with pulmonary tuberculosis. *Microbiome* **2**, 29 (2014).

27. Cui, Z. *et al.* Complex sputum microbial composition in patients with pulmonary tuberculosis. *BMC Microbiol.* **12**, 276 (2012).

28. Cheung, M. K. *et al.* Sputum Microbiota in Tuberculosis as Revealed by 16S rRNA Pyrosequencing. *PLoS One* **8**, e54574 (2013).

29. Hu, Y. *et al.* Metagenomic analysis of the lung microbiome in pulmonary tuberculosis - a pilot study. *Emerg. Microbes Infect.* **9**, 1444–1452 (2020).

30. Keegan, K. P., Glass, E. M. & Meyer, F. MG-RAST, a metagenomics service for analysis of microbial community structure and function. in *Methods in Molecular Biology* **1399**, 207–233 (Humana Press Inc., 2016).

31. McMurdie, P. J. & Holmes, S. Phyloseq: An R Package for Reproducible Interactive Analysis and Graphics of Microbiome Census Data. *PLoS One* **8**, e61217 (2013).

32. Kateete, D. P. *et al.* Sputum microbiota profiles of treatment-naïve TB patients in Uganda before and during first-line therapy. *bioRxiv* (2020). doi:10.1101/2020.04.24.20078246

33. Enagbonma, B. J., Amoo, A. E. & Babalola, O. O. Deciphering the microbiota data from termite mound soil in South Africa using shotgun metagenomics. *Data Br.* **28**, (2020).

34. Delmont, T. O. *et al.* Structure, fluctuation and magnitude of a natural grassland soil metagenome. *ISME J.* **6**, 1677–1687 (2012).

35. Soriano, B. M., Del Valle-Perez, L. M., Morales-Vale, L. & Rios-Velazquez, C. Datasets generated by shotgun sequencing of metagenomic libraries of the guajataca water reservoir. *Data Br.* **21**, 2531–2535 (2018).

36. Sharma, S. *et al.* Transcriptome analysis of mycobacteria in sputum samples of pulmonary tuberculosis patients. *PLoS One* **12**, 1–16 (2017).

37. Maiga, M. *et al.* Stool microbiome reveals diverse bacterial ureases as confounders of oral urea breath testing for Helicobacter pylori and Mycobacterium tuberculosis in Bamako, Mali. *J. Breath Res.* **10**, 36012 (2016).

38. Vázquez-Pérez, J. A. *et al.* Alveolar microbiota profile in patients with human pulmonary tuberculosis and interstitial pneumonia. *Microb. Pathog.* **139**, 103851 (2020).

39. Wu, J. *et al.* Sputum microbiota associated with new, recurrent and treatment failure tuberculosis. *PLoS One* **8**, e83445 (2013).

40. Krishna, P., Jain, A. & Bisen, P. S. Microbiome diversity in the sputum of patients with pulmonary tuberculosis. *Eur. J. Clin. Microbiol. Infect. Dis.* **35**, 1205–1210 (2016).

41. Lin, D. *et al.* Sputum microbiota as a potential diagnostic marker for multidrug-resistant tuberculosis. *Int. J. Med. Sci.* **18**, 1935–1945 (2021).

42. Osei Sekyere, J. & Asante, J. Emerging mechanisms of antimicrobial resistance in bacteria and fungi: advances in the era of genomics. *Future Microbiol.* **13**, 241–262 (2018).

693 **Figure 1.** Demographic information and sputum sampling of recruited patients. The patients
694 were aged between 23 and 55 years, with a median age of 38 years and average age of 37.41
695 years (**A**). Six of the patients were females whilst 15 were males, with the females and males
696 having a respective mean age of 30.60 and 40.25 years (**B**). Sputum samples collected at
697 baseline, day 1, day 2, and day 7 were obtained from 7 patients whilst three patients provided
698 samples at baseline, day 1, and day 2, and one patient provided only baseline and day 7
699 sputum samples (**C**). Only nine of the 11 sequenced reads qualified for inclusion in
700 downstream analysis owing to their higher coverage (>10X) (**D**).

701 **Figure 2. Count and abundance of genera OTU per sample, and alpha and beta**
702 **diversities.** The total abundance of genera OTUs across all samples shows that 104D0 and
703 108D0 had the highest OTU abundance. Only a few genera had significant (t-test) abundance
704 variation across each sample: 104D1 (p: 0.031), 105D2 (p: 0.2376), 107D2 (p: 0.007), 108D2
705 (p: 0.0114), 109D2 (p: 0.0178) (**A)**. Wilcoxon's test found all genera abundance to be
706 significant (p: <0.0001), but they were insignificant by t-test; one- & two-way ANOVA were
707 both significant. The count of all genera (OTUs) per sample shows sample 108D0 had the
708 highest number of genera; count per genera was statistically significant (p: <0.0001) (**B**).
709 Alpha-diversity of each sample is shown in **C** and they were all significant (p: <0.0001**).** The
710 β-diversities between samples of the same patient are shown in **D**, with the variations
711 between β-diversities varying per patient (p: <0.0001). β-diversity between baseline (S1) and
712 day 1 (S2) is shown as blue bars, between baseline and day 2 (S3) is shown as orange bars,
713 between baseline and day 7 (S4) is shown as grey bars, between days 1 (S2) and 2 (S3) is
714 shown as yellow bars, between days 1 and 7 is shown as light blue bars, and between days 2
715 and 7 are shown as green bars. The β-diversity variations between samples collected at the
716 same time point (days 0, 1, 2, and 7) from different patients is shown in **E** (p: 0.0821;
717 <0.0001). S1, S2, S3, and S4 represent days 0 (baseline), 1, 2, and 7 respectively. The β-

diversity variation between samples collected at the same time points, but from different patients, are shown as coloured bars: blue (baseline), orange (day 1), grey (day 2) and yellow (day 7).

Figure 3. Total abundance of taxonomic Kingdoms per sample. Bacteria was most dominant across all samples except in 107D2, 109D1, 109D2, where Fungi was most dominant. Parasites were also found in substantial proportions in 104D1, 105D2, 107D7, 108D1, 108D2, 109D1, 109D2, and 112D2, but viruses and archaea were very minor in abundance in all the samples. Wilcoxon's test showed significance (p: <0.0001) for all kingdoms and 2-Way ANOVA was significant for the samples (**A**). Among almost all the samples, the bacterial phylum Firmicutes was the most dominant, except in 105D2, 107D2, 108D1, and 112D2 where it was almost absent. Actinobacteria was the next dominant phylum, with Proteobacteria, Bacteroidetes and the other phyla occupying a relatively small portion of the microbiota. A reduction in bacterial phyla abundance was seen after the baseline until on day 7, when a rise in abundance was observed again in all the samples (**B**).

Figure 4. Abundance and diversity of OTUs in Firmicutes, Proteobacteria, Actinobacteria, Bacteroides and other bacterial orders in sputum samples. A u-shaped pattern was observed among genera in the various phyla: they reduced in abundance after day 0 and rose gradually from day 2 to day 7. The diversities reduced or increased depending on the patient. The abundance and diversity of genera found in the phylum Firmicutes is shown in **A**; Streptococcus was the commonest genus and reduced after baseline but rose gradually from day 2 unto day 7. This u-shaped pattern was observed in other genera under Firmicutes. Abundance and diversity of genera under Proteobacteria are shown in **B**, in which Pseudomonas was the most abundant. Among Actinobacteria (**C**), Mycobacterium was common, but also reduced drastically after the baseline and hardly rose again, making it the genera most affected by the antibiotics. Bacteroidetes, Cyanobacteria, Tenericutes and other

743 Phyla with relatively little abundance are shown in **D**. Within these phyla, the u-shaped
744 pattern was also observed from baseline to day 7, with days 1 and 2 having lower
745 abundances.

746 **Figure 5. Abundance of selected genera in all samples across different sampling-time**
747 **points.** The abundance of Streptococcus (**A**), Mycobacterium (**B**), and different sets of
748 selected genera (**C, D, E**, and **F**) across different sampling-time points (baseline, day 1, day
749 2, and day 7) showed a reduction in abundance after baseline on days 1 and 2, and a rise on
750 day 7. However, Mycobacterium declined after the baseline and continued declining
751 afterwards. The variations in abundance over sampling time was significant for Streptococcus
752 (p: 0.0078) Granulicatella (p: 0.0432), Clostridium, Lactobacillus (p: 0.0272),
753 Bifidobacterium (p: 0.0071), Bacillus (0.0141) etc. by one-sample t-test, and was significant
754 for almost all the selected genera, including Mycobacterium (p: <0.0001). One-/two-way
755 ANOVA matching of the genera to their abundance were significant (Dataset 3).

756 **Figure 6. Abundance of archaea, parasite, fungi, and viral OTUs per sample.** The
757 abundance of archaeal OTUs is shown in **A**, where only 108D0 had 4 archaeal genera; Two-
758 way ANOVA was significant for only the row factor. Both Wilcoxon's and one-sample t-
759 tests were insignificant. Abundance of parasites per sample is shown in **B**; parasites were
760 found in all samples with non-consistent variations in abundance across different sampling-
761 time points per patient. Two-way ANOVA column factor was significant. Schistosoma
762 (p:0.0014), Moniezia (p:0.0187), Drosophila (p:0.0406), Plasmodium (p:0.0404), &
763 Monosiga (p:0.0256) were significant by one-sample & Wilcoxons' tests; Noniella (p:0.0005)
764 & Codonosigidae (p:<0.0001) were only significant with Wilcoxon's test. The abundance and
765 variations of 51 fungal OTUs across different sampling-times per patient is shown in **C**; 2-
766 Way ANOVA of fungi genera with abundance was insignificant. Also, none of the
767 abundance variations in any of the fungal genera were significant except Saccharomyces

(p:0.0078) & Penicillium (p:0.0078)**.** Siphoviridae, Podoviridae, Myoviridae, Retroviridae, Anelloviridae, T4-like, Muromegalovirus, Caudovirales, and Lymphocryptovirus viruses were the viruses found in mainly baseline and day 7 samples, with 107D2 and 111D1 being the only samples from days 2 and 1, respectively (**D**). Although the presence of viruses in the samples were significant (2-Way ANOVA), none of the variations in abundance for every virus OTU was significant.

Figure 7. Functional component subsystem distribution per sample. The functional composition of each sample is shown in **A**, where clustering-based subsystems, carbohydrates, protein metabolism etc., dominated the samples. The samples with the most abundant functional subsystems components were mainly baseline and day 7 samples such as 104D0, 108D0, 108D7, 111D7, 112D0, 109D7, 107D7, and 107D0 (**B**). A sampling time-point grouping shows that baseline and day 7 samples had the most functional components whilst days 1 and 2 samples had lower functional components (**C**). U-shaped patterns were observed across the sampling points, with abundance of functional components reducing from baseline to days 1 and 2, and increasing on day 7 (**D**). Functional subsystems components with the most substantial proportion in all the samples shows that clustering-based subsystems, carbohydrates, protein metabolism, RNA metabolism, amino acids and derivates, and DNA metabolism were common subsystems. These varied across the samples at different sampling points: baseline, day 1, day 2, and day 7 (**E**). The variations in abundance for the functional components of each sample was statistically significant; two-way ANOVA was significant.

Figure 8. Nonmetric multidimensional scaling (NMDS) and ordination plots. The microbiota were closely related to each other at baseline, but became less related/connected at days 1 and 2; the networks between the microbiota increased at day7. The network analysis of the microbiota between baseline and day 2 is shown in **A** and **B** respectively. The

ordination plots showing the spatial relationship between the microbiota are shown in **C** and **D** respectively.

Dataset 1. Patient demographics, sputum sampling, and sputum characteristics

Dataset 2. Operational taxonomic units (OTU) abundance per sputum sample, taxonomy, metadata, resistance mechanisms and mobile genetic elements in each sputum sample.

Dataset 3. Statistical analyses of microbiome OTU data per sample.

Figure S1. Total OTU abundance of the various genera across all samples. The total abundance of each OTU genera across all samples are categorised into four: above 1000 (**A**), between 1000-100 (**B**), between 100-10 (**C**), and below 10 (**D**). Most genera were below 10 and a few were above 1000.

Figure S2. Chao1 and Shannon alpha diversities of samples according to daily collections and OTU genera categorisation. The Chao1 and Shannon indices differed from each other for the same sample and patient.

Figure S3. Abundance of each taxonomic rank, from kingdom to genus, in each sample. A detailed breakdown of each kingdom, phylum, class, order, family, and genus in each sample across all time points and in only baseline, day 1, 2, and 7 samples are shown in i to xxx.

Figure S4. Abundance of bacterial OTUs per taxonomic rank and sampling-time point per sample. Common bacterial genera included Streptococci, Mycobacterium, Veillonella, and Pseudomonas. Abundance of each OTU per taxonomic rank and sampling time-points shows antibiotic-mediated variations from baseline to day 7.

Figure S5. Abundance of parasite OTUs per taxonomic rank and sampling-time point per sample.

Figure S6. Abundance of fungi OTUs per taxonomic rank and sampling-time point per sample.

Figure S7. Abundance of viral OTUs per taxonomic rank and sampling-time point per sample.

Figure S8. Functional components and subsystems of the various samples. The functional components and subsystems shifted in proportion per sample for the different sampling points.

Figure S9. Network analysis showing the spatial interactions and networking of the various microbial components in the sputum microbiota.

Figure S10. Non-metric multidimensional scaling (NMDS) of the various OTUs showing their ordination plots and spatial orientation per kingdom.

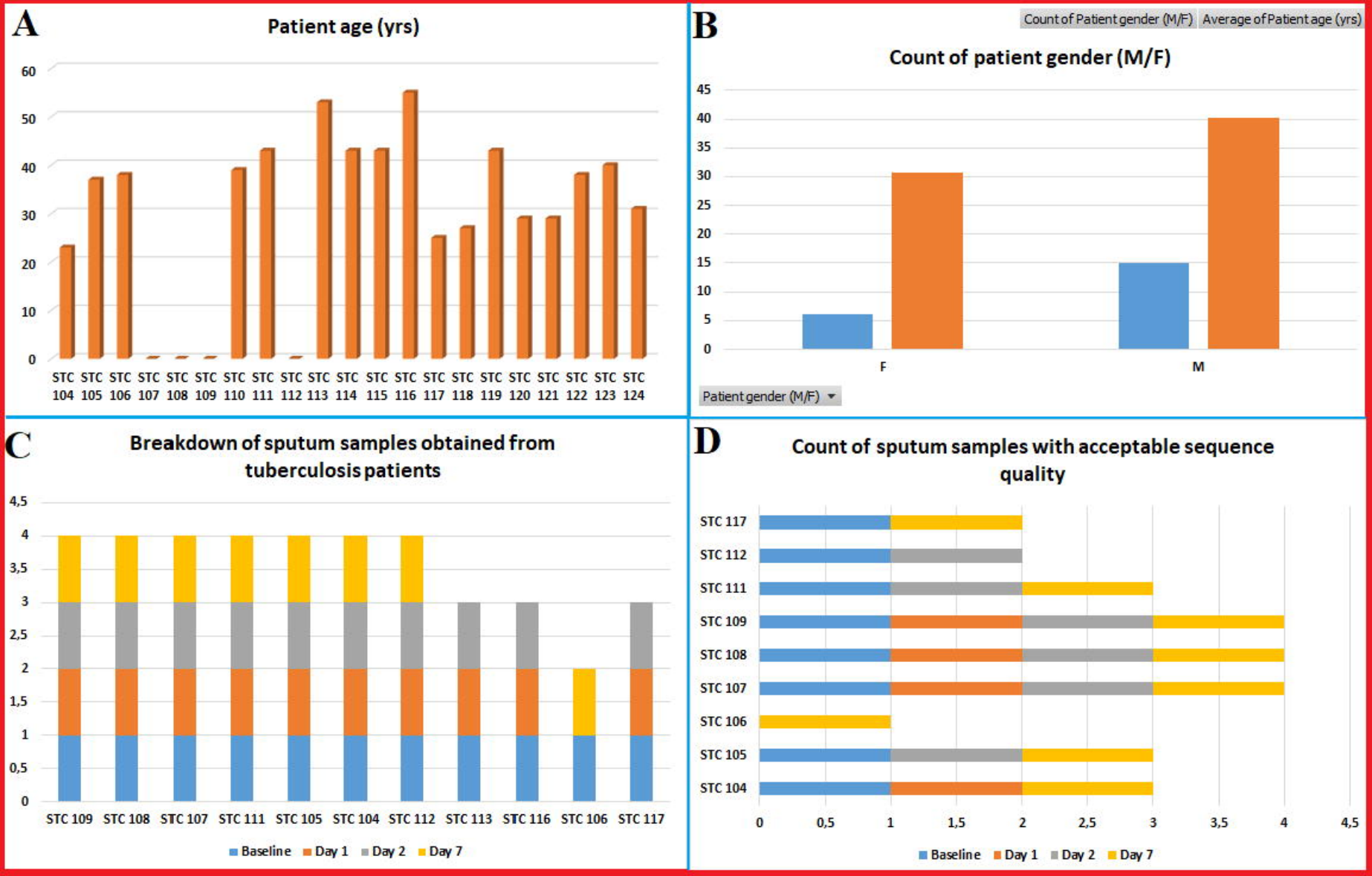
A
Patient age (yrs)
60
50
40
30
20
10
0
STC 104
STC 105
STC 106
STC 107
STC 108
STC 109
STC 110
STC 111
STC 112
STC 113
STC 114
STC 115
STC 116
STC 117
STC 118
STC 119
STC 120
STC 121
STC 122
STC 123
STC 124
B
Count of Patient gender (M/F)
Average of Patient age (yrs)
Count of patient gender (M/F)
45
40
35
30
25
20
15
10
5
0
F
M
Patient gender (M/F)
C
Breakdown of sputum samples obtained from tuberculosis patients
4,5
4
3,5
3
2,5
2
1,5
1
0,5
0
STC 109
STC 108
STC 107
STC 111
STC 105
STC 104
STC 112
STC 113
STC 116
STC 106
STC 117
Baseline
Day 1
Day 2
Day 7
D
Count of sputum samples with acceptable sequence quality
STC 117
STC 112
STC 111
STC 109
STC 108
STC 107
STC 106
STC 105
STC 104
0
0,5
1
1,5
2
2,5
3
3,5
4
4,5
Baseline
Day 1
Day 2
Day 7


A
Genera abundance per sample
Abundance
Patients' sputum samples
B
Count of total genera in sample
Count
Patients' sputum samples
C
Alpha-diversity per sample
Alpha-diversity
Patients' sputum samples
D
Within-host β-diversities between samples
β-diversities
Sputum samples from patients
(S1-c)+(S2-c)
(S1-c)+(S3-c)
(S1-c)+(S4-c)
(S2-c)+(S3-c)
(S2-c)+(S4-c)
(S3-c)+(S4-c)
E
Interpatient β-diversities
β-diversities
Inter-patient sputum samples
(S1-c)+(S1-c)
(S2-c)+(S2-c)
(S3-c)+(S3-c)
(S4-c)+(S4-c)

A

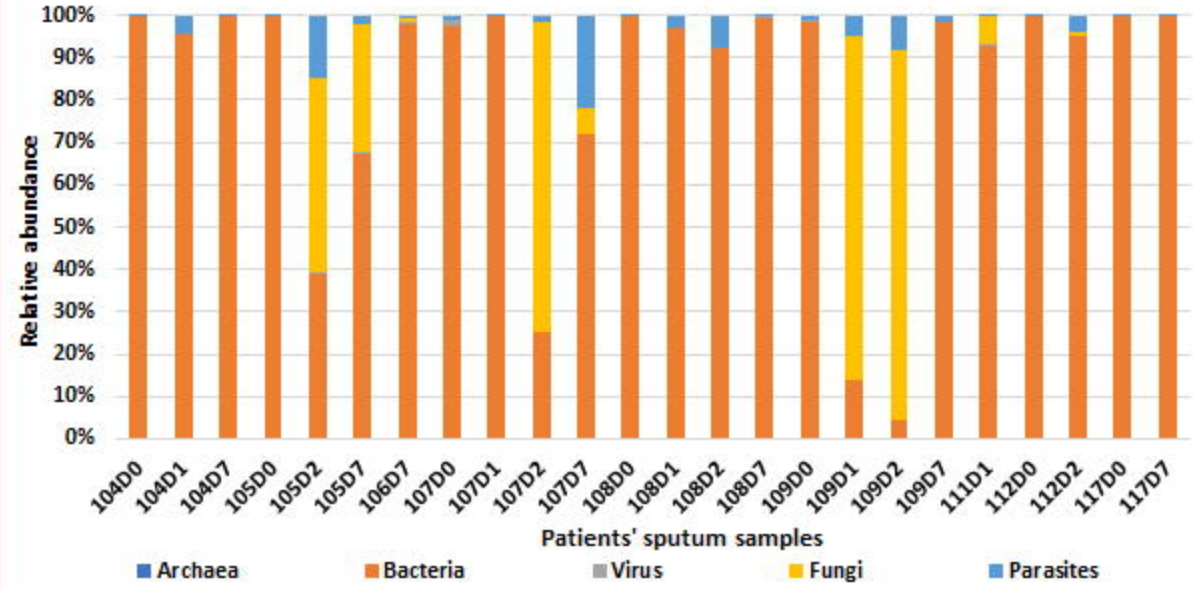
Total abundance of Kingdoms per sample
Relative abundance
100%
90%
80%
70%
60%
50%
40%
30%
20%
10%
0%
104D0
104D1
104D7
105D0
105D2
105D7
106D7
107D0
107D1
107D2
107D7
108D0
108D1
108D2
108D7
109D0
109D1
109D2
109D7
111D1
112D0
112D2
117D0
117D7
Patients' sputum samples
Archaea
Bacteria
Virus
Fungi
Parasites

B

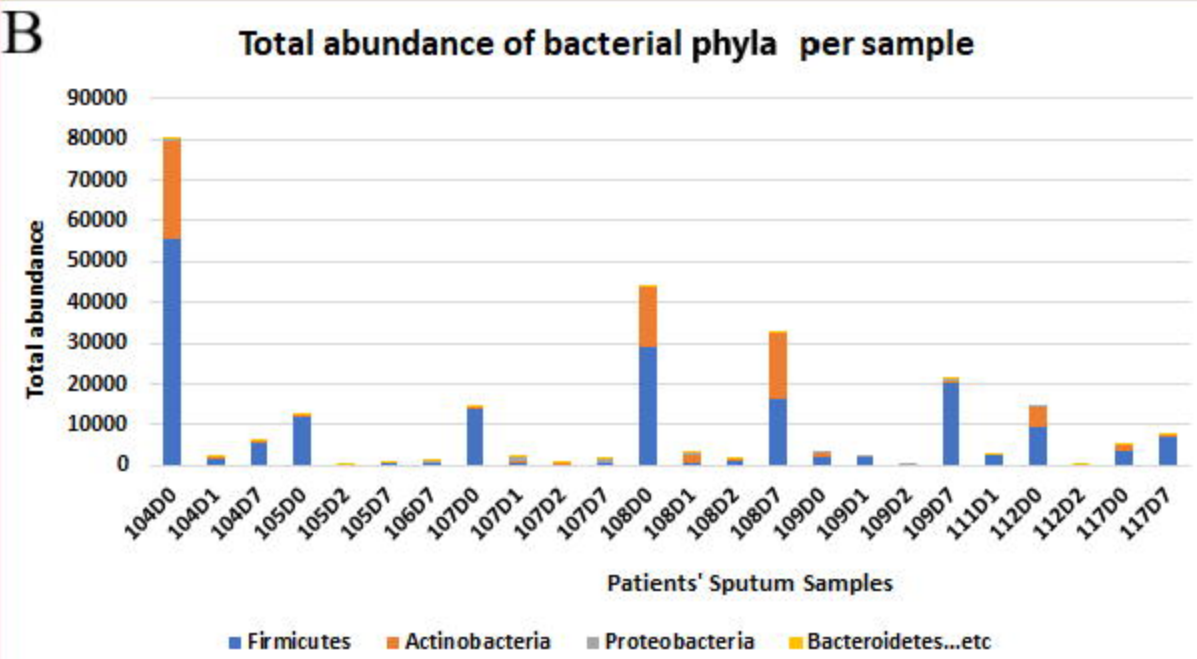
Total abundance of bacterial phyla per sample
Total abundance
90000
80000
70000
60000
50000
40000
30000
20000
10000
0
104D0
104D1
104D7
105D0
105D2
105D7
106D7
107D0
107D1
107D2
107D7
108D0
108D1
108D2
108D7
109D0
109D1
109D2
109D7
111D1
112D0
112D2
117D0
117D7
Patients' Sputum Samples
Firmicutes
Actinobacteria
Proteobacteria
Bacteroidetes...etc


A
Relative abundance of Firmicutes in patients with tuberculosis
Relative abundance
100%
80%
60%
40%
20%
0%
104D0 104D1 104D7 105D0 105D2 105D7 106D7 107D0 107D1 107D2 107D7 108D0 108D1 108D2 108D7 109D0 109D1 109D2 109D7 111D1 112D0 112D2 117D0 117D7
Patients' sputum samples
Streptococcus
Clostridium
Bacillus
Staphylococcus
Oribacterium
Solobacterium
Peptoniphilus
Selenomonas
Paenibacillus
Blautia
Megamonas
Brevibacillus
Geobacillus
Eremococcus
Pediococcus
Anaerostipes
Carboxydothermus
Acidaminococcus
Unclassified (derived from Firmicutes)
Atopobium
Gemella
Ruminococcus
Unclassified (Clostridiales Family XI. Incertae Sedis)
Shuttleworthia
Coprobacillus
Listeria
unclassified (derived from Lachnospiraceae)
Thermosinus
Ammonifex
Mitsuokella
Turicibacter
Alicyclobacillus
Carnobacterium
Alkaliphilus
Butyrivibrio
Thermosediminibacter
Halanaerobium
Catonella
Lactobacillus
Enterococcus
Veillonella
unclassified (derived from Erysipelotrichaceae)
Roseburia
Leuconostoc
Treponema
Abiotrophia
Catenibacterium
Anaerococcus
Lysinibacillus
Macrococcus
Trichococcus
Finegoldia
Desulfotomaculum
Erysipelothrix
Filifactor
Eubacterium
Unclassified (derived from Clostridiales)
Lactococcus
Peptostreptococcus
Coprococcus
Bulleidia
Weissella
Cardiobacterium
Faecalibacterium
Phascolarctobacterium
Thermincola
Subdoligranulum
Aerococcus
Tetragenococcus
Pseudoramibacter
Anaerotruncus
Holdemania
Heliobacterium
B
Abundance of Proteobacteria in patients with tuberculosis
Abundance
1200
1000
800
600
400
200
0
104D0 104D1 104D7 105D0 105D2 105D7 106D7 107D0 107D1 107D2 107D7 108D0 108D1 108D2 108D7 109D0 109D1 109D2 109D7 111D1 112D0 112D2 117D0 117D7
Patients' sputum samples
Neisseria
Psychrobacter
Methylobacter
Lautropia
Sinorhizobium
Burkholderia
Aurantimonas
Dickeya
Rhizobium
Janthinobacterium
Enterobacter
Proteus
Mannheimia
Alicycliphilus
Francisella
unclassified (derived from Alphaproteobacteria)
Oceanicola
unclassified (derived from Rhodobacteraceae)
Desulfobulbus
Hahella
Achromobacter
Escherichia
Stenotrophomonas
Desulfomicrobium
Ochrobactrum
Ralstonia
Candidatus Pelagibacter
Salmonella
Sphingomonas
Thiobacillus
Erwinia
Serratia
Azotobacter
Marinobacter
Enhydrobacter
Agrobacterium
Arsenophonus
unclassified (derived from Rhodobacterales)
Nitrosomonas
Roseovarius
Pseudomonas
Methylotenera
unclassified (derived from Gammaproteobacteria)
Methylobacterium
Bordetella
Acidovorax
Kingella
Marinomonas
Polaromonas
Halliangium
Klebsiella
Shigella
unclassified (derived from Vibrionales)
Eikenella
Histophilus
Cronobacter
Shewanella
Erythrobacter
Citrobacter
Anaeromyxobacter
Haemophilus
Gluconacetobacter
Cardiobacterium
Cupriavidus
Rhodopseudomonas
Variovorax
Laribacter
Vibrio
Verminephrobacter
Pseudoalteromonas
Pantoea
Legionella
Xanthomonas
Beggiatoa
Halomonas
Loktanella
Helicobacter
Campylobacter
unclassified (derived from Campylobacterales)
C
Relative abundance of Actinobacteria in patients with tuberculosis
Abundance
30000
25000
20000
15000
10000
5000
0
104D0 104D1 104D7 105D0 105D2 105D7 106D7 107D0 107D1 107D2 107D7 108D0 108D1 108D2 108D7 109D0 109D1 109D2 109D7 111D1 112D0 112D2 117D0 117D7
Sputum sample per patient
Mycobacterium
Corynebacterium
Arthrobacter
Brevibacterium
Frankia
Nocardiopsis
Eggerthella
Atopobium
Propionibacterium
Nocardia
Arcanobacterium
Stackebrandtia
Xylanimonas
Gardnerella
Actinomyces
Scardovia
Parascardovia
Intrasporangium
Sanguibacter
Amycolatopsis
Geodermatophilus
Rothia
Nakamurella
Conexibacter
Cellulomonas
Jonesia
Kitasatospora
Janibacter
Bifidobacterium
Beutenbergia
Actinosynnema
Brachybacterium
Kineococcus
Microbispora
Mobiluncus
Kocuria
Gordonia
Dermacoccus
Saccharomonospora
Nonomuraea
Olsenella
Rhodococcus
Micromonospora
Pseudonocardia
Micrococcus
Streptosporangium
Collinsella
Segniliparus
Cryptobacterium
Kytococcus
Renibacterium
Tsukamurella
Slackia
Streptomyces
Gordoniacter
Dietzia
Nocardioides
Tropheryma
D
Abundance of Bacteroides, Cyanobacteria, Tenericutes & other phyla in patients with tuberculosis
Abundance
600
500
400
300
200
100
0
104D0 104D1 104D7 105D0 105D2 105D7 106D7 107D0 107D1 107D2 107D7 108D0 108D1 108D2 108D7 109D0 109D1 109D2 109D7 111D1 112D0 112D2 117D0 117D7
Patients' sputum samples
Prevotella
Nostoc
Synechococcus
Algoriphagus
Trichodesmium
Tannerella
Blattabacterium
Deinococcus
Spirochaeta
unclassified (derived from Cyanobacteria)
Fusobacterium
Pyramidobacter
Nodularia
Spirosoma
Acaryochloris
Dehalogenimonas
unclassified (derived from Bacteroidetes)
Fibrobacter
Leptospirillum
Dyadobacter
Bacteroides
Anabaena
Microcoleus
Mucilaginibacter
unclassified (derived from Synergistetes)
Jonquetella
Prosthecochloris
Methylacidiphilum
Thermodesulfovibrio
Acholeplasma
Candidatus Phytoplasma
Aminobacterium
Oscillatoria
Roseiflexus
Treponema
Sebaldella
Ktedonobacter
Coraliomargarita
Planctomyces
Cyanothece
Chitinophaga
Porphyromonas
Cylindrospermopsis
Hydrogenobacter
Parabacteroides
Gloeobacter
Mycoplasma
Rhodothermus

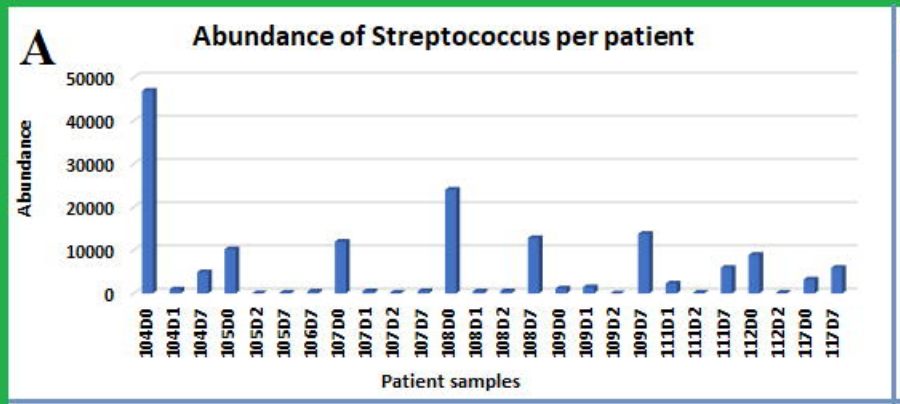
A
Abundance of Streptococcus per patient
Abundance
Patient samples

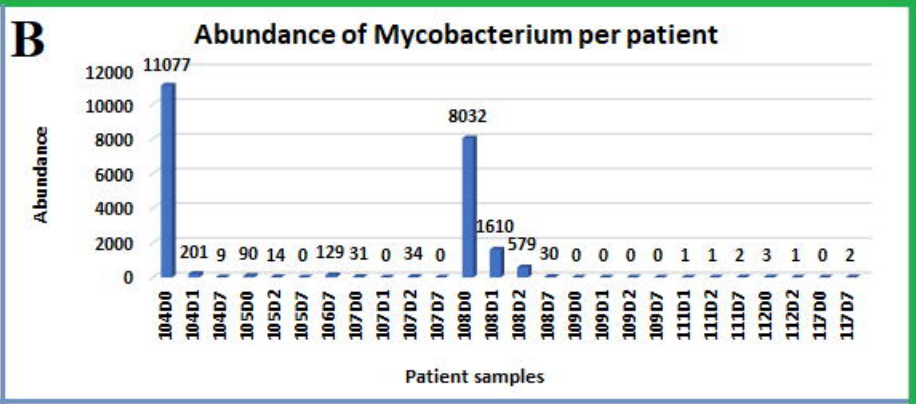
B
Abundance of Mycobacterium per patient
11077
8032
1610
579
Abundance
Patient samples

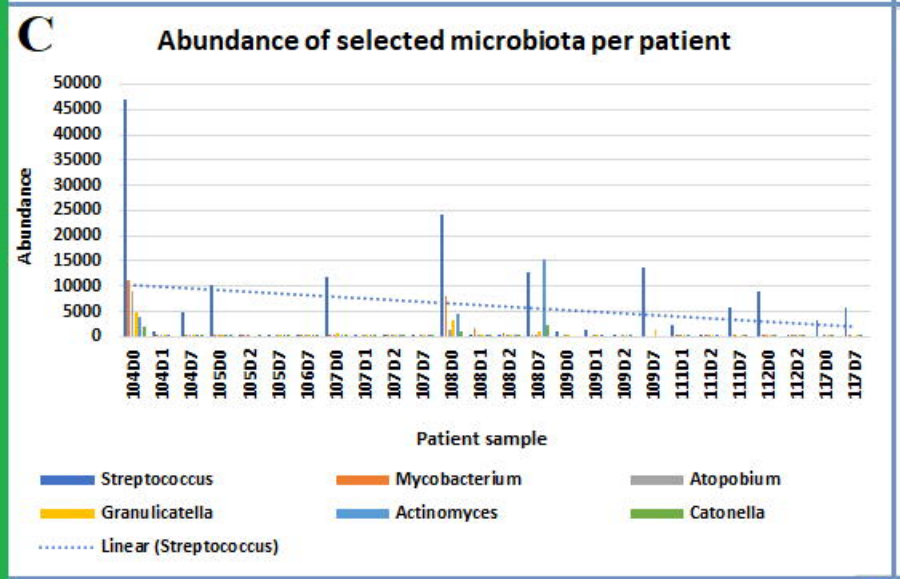
C
Abundance of selected microbiota per patient
Abundance
Patient sample
Streptococcus
Mycobacterium
Atopobium
Granulicatella
Actinomyces
Catonella
Linear (Streptococcus)

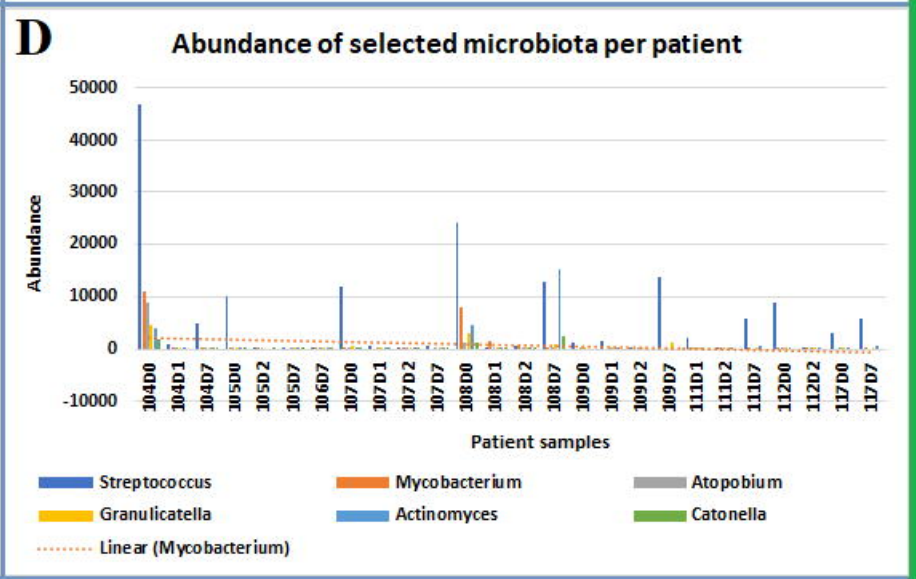
D
Abundance of selected microbiota per patient
Abundance
Patient samples
Streptococcus
Mycobacterium
Atopobium
Granulicatella
Actinomyces
Catonella
Linear (Mycobacterium)

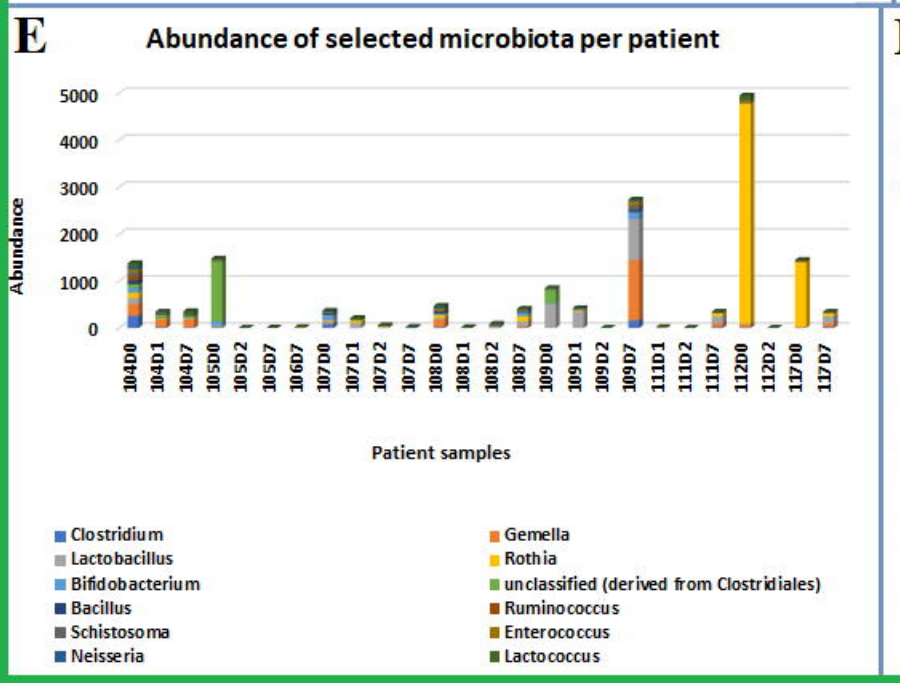
E
Abundance of selected microbiota per patient
Abundance
Patient samples
Clostridium
Lactobacillus
Bifidobacterium
Bacillus
Schistosoma
Neisseria
Gemella
Rothia
unclassified (derived from Clostridiales)
Ruminococcus
Enterococcus
Lactococcus

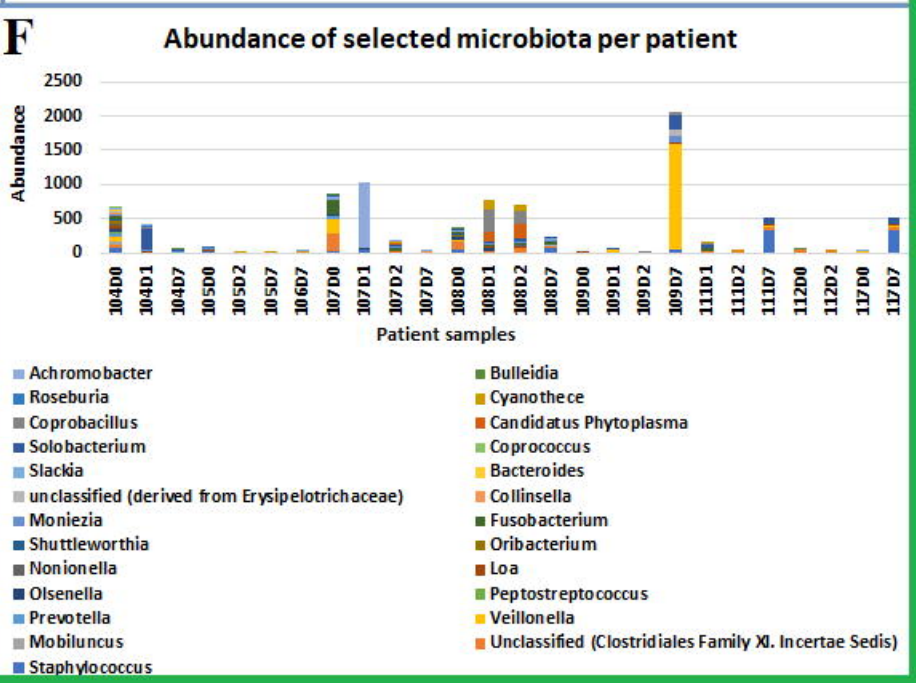
F
Abundance of selected microbiota per patient
Abundance
Patient samples
Achromobacter
Roseburia
Coprobacillus
Solobacterium
Slackia
unclassified (derived from Erysipelotrichaceae)
Moniezia
Shuttleworthia
Nonionella
Olsenella
Prevotella
Mobiluncus
Staphylococcus
Bulleidia
Cyanothece
Candidatus Phytoplasma
Coprococcus
Bacteroides
Collinsella
Fusobacterium
Oribacterium
Loa
Peptostreptococcus
Veillonella
Unclassified (Clostridiales Family XI. Incertae Sedis)

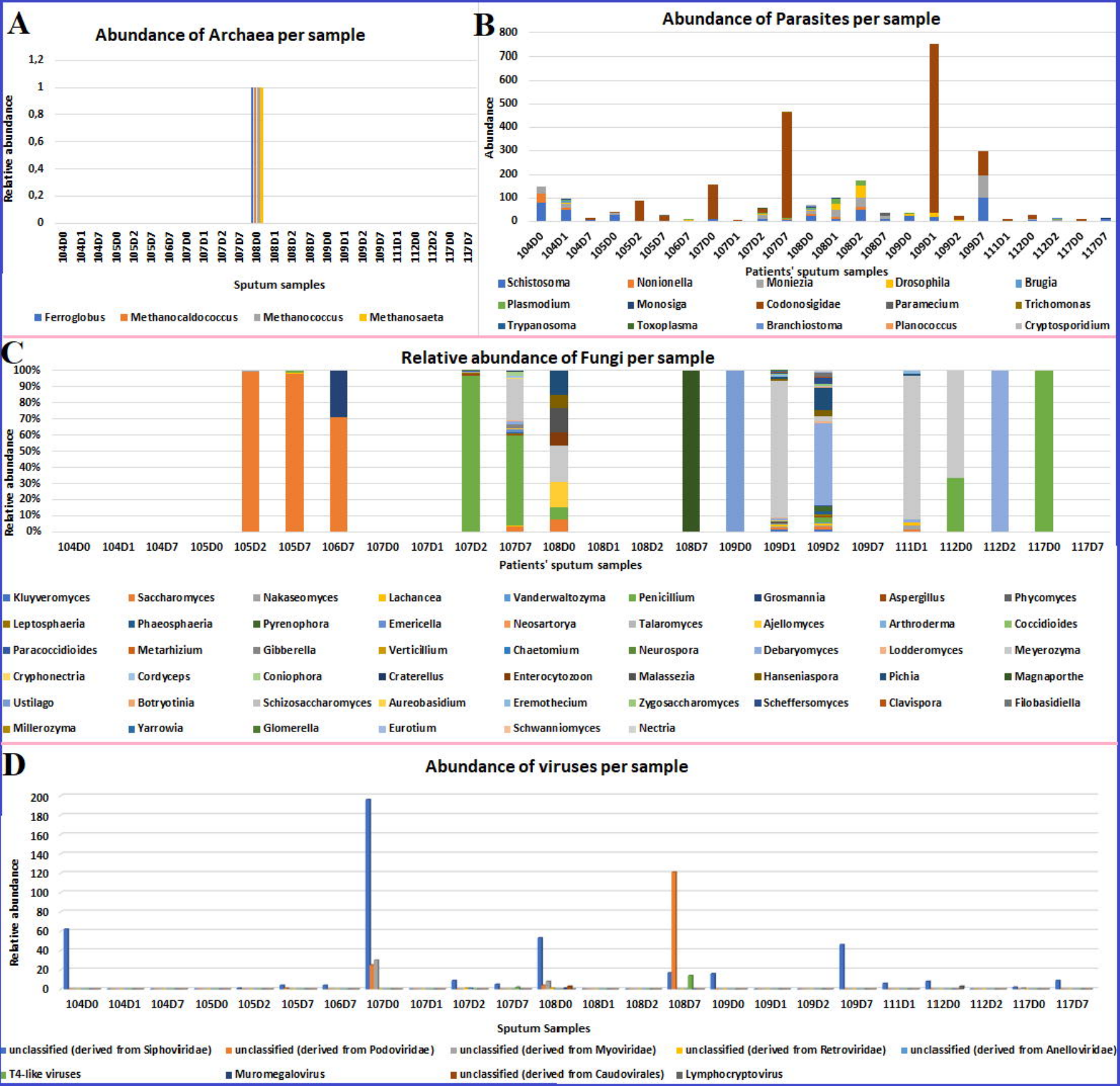
A
Abundance of Archaea per sample
Relative abundance
1,2
1
0,8
0,6
0,4
0,2
0
104D0 104D1 104D7 105D0 105D2 105D7 106D7 107D0 107D1 107D2 107D7 108D0 108D1 108D2 108D7 109D0 109D1 109D2 109D7 111D1 112D0 112D2 117D0 117D7
Sputum samples
Ferroglobus
Methanocaldococcus
Methanococcus
Methanosaeta
B
Abundance of Parasites per sample
Abundance
800
700
600
500
400
300
200
100
0
104D0 104D1 104D7 105D0 105D2 105D7 106D7 107D0 107D1 107D2 107D7 108D0 108D1 108D2 108D7 109D0 109D1 109D2 109D7 111D1 112D0 112D2 117D0 117D7
Patients' sputum samples
Schistosoma
Nonionella
Moniezia
Drosophila
Brugia
Plasmodium
Monosiga
Codonosigidae
Paramecium
Trichomonas
Trypanosoma
Toxoplasma
Branchiostoma
Planococcus
Cryptosporidium
C
Relative abundance of Fungi per sample
Relative abundance
100%
90%
80%
70%
60%
50%
40%
30%
20%
10%
0%
104D0 104D1 104D7 105D0 105D2 105D7 106D7 107D0 107D1 107D2 107D7 108D0 108D1 108D2 108D7 109D0 109D1 109D2 109D7 111D1 112D0 112D2 117D0 117D7
Patients' sputum samples
Kluyveromyces
Saccharomyces
Nakaseomyces
Lachancea
Vanderwaltozyma
Penicillium
Grosmannia
Aspergillus
Phycomyces
Leptosphaeria
Phaeosphaeria
Pyrenophora
Emericella
Neosartorya
Talaromyces
Ajellomyces
Arthroderma
Coccidioides
Paracoccidioides
Metarhizium
Gibberella
Verticillium
Chaetomium
Neurospora
Debaryomyces
Lodderomyces
Meyerozyma
Cryphonectria
Cordyceps
Coniophora
Craterellus
Enterocytozoon
Malassezia
Hanseniaspora
Pichia
Magnaporthe
Ustilago
Botryotinia
Schizosaccharomyces
Aureobasidium
Eremothecium
Zygosaccharomyces
Scheffersomyces
Clavispora
Filobasidiella
Millerozyma
Yarrowia
Glomerella
Eurotium
Schwanniomyces
Nectria
D
Abundance of viruses per sample
Relative abundance
200
180
160
140
120
100
80
60
40
20
0
104D0 104D1 104D7 105D0 105D2 105D7 106D7 107D0 107D1 107D2 107D7 108D0 108D1 108D2 108D7 109D0 109D1 109D2 109D7 111D1 112D0 112D2 117D0 117D7
Sputum Samples
unclassified (derived from Siphoviridae)
unclassified (derived from Podoviridae)
unclassified (derived from Myoviridae)
unclassified (derived from Retroviridae)
unclassified (derived from Anelloviridae)
T4-like viruses
Muromegalovirus
unclassified (derived from Caudovirales)
Lymphocryptovirus

A

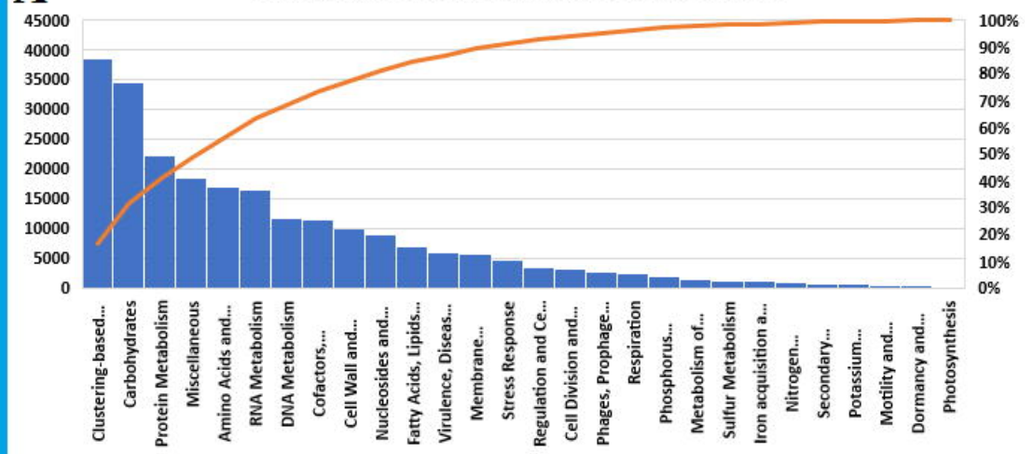
Functional components of all sputum samples
Clustering-based...
Carbohydrates
Protein Metabolism
Miscellaneous
Amino Acids and...
RNA Metabolism
DNA Metabolism
Cofactors,...
Cell Wall and...
Nucleosides and...
Fatty Acids, Lipids...
Virulence, Diseas...
Membrane...
Stress Response
Regulation and Ce...
Cell Division and...
Phages, Prophage...
Respiration
Phosphorus...
Metabolism of...
Sulfur Metabolism
Iron acquisition a...
Nitrogen...
Secondary...
Potassium...
Motility and...
Dormancy and...
Photosynthesis

B

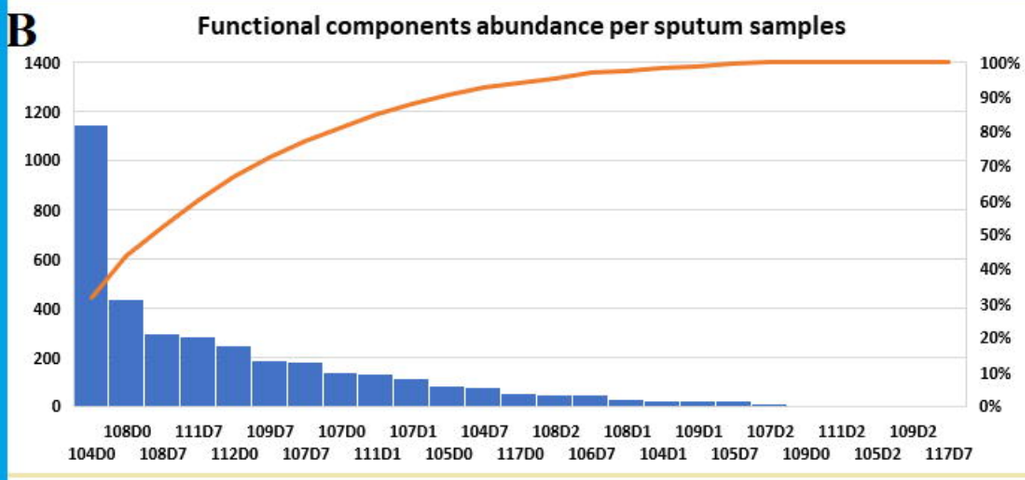
Functional components abundance per sputum samples
108D0 111D7 109D7 107D0 107D1 104D7 108D2 108D1 109D1 107D2 111D2 109D2
104D0 108D7 112D0 107D7 111D1 105D0 117D0 106D7 104D1 105D7 109D0 105D2 117D7

C

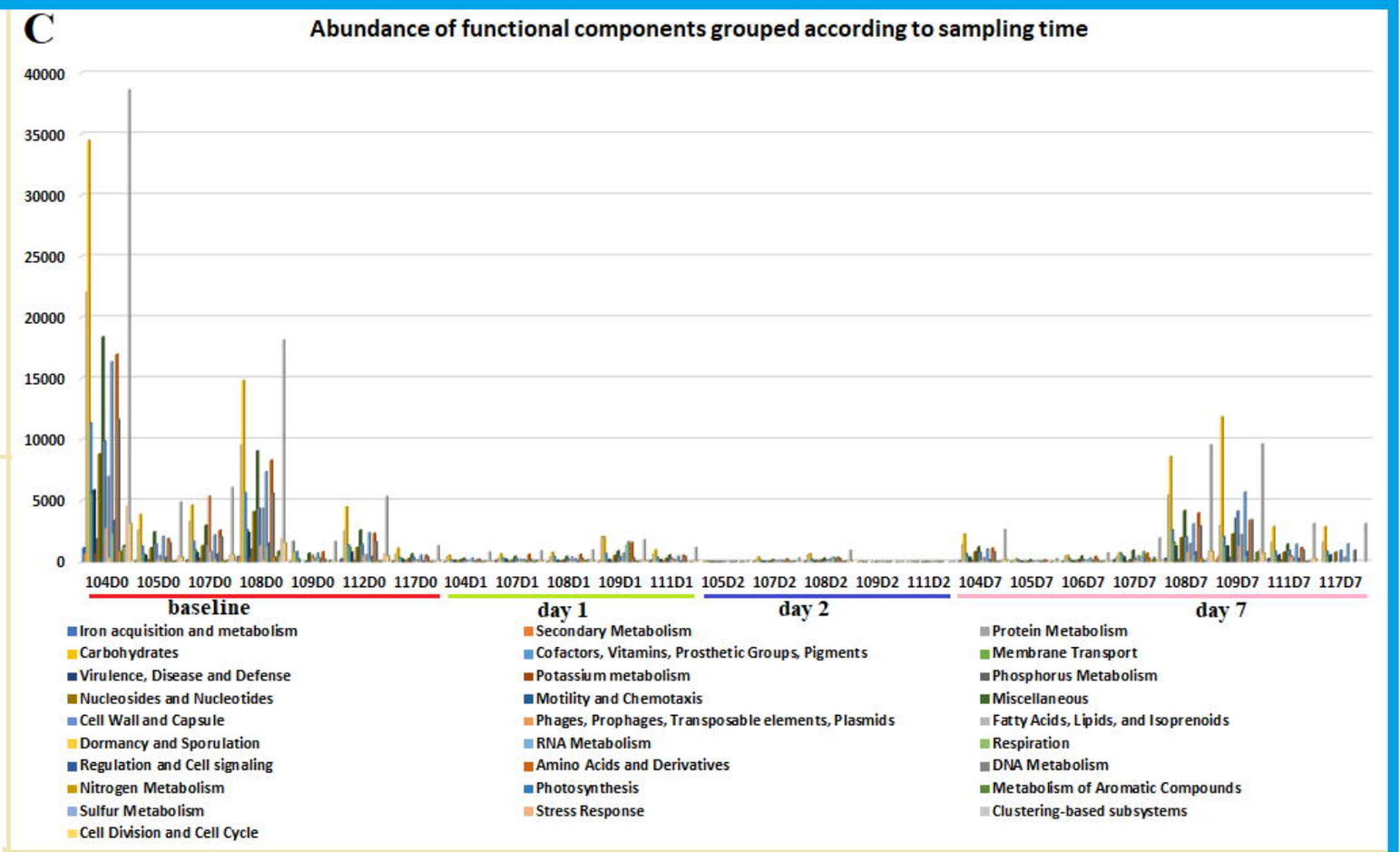
Abundance of functional components grouped according to sampling time
104D0 105D0 107D0 108D0 109D0 112D0 117D0 104D1 107D1 108D1 109D1 111D1 105D2 107D2 108D2 109D2 111D2 104D7 105D7 106D7 107D7 108D7 109D7 111D7 117D7
baseline
day 1
day 2
day 7
Iron acquisition and metabolism
Carbohydrates
Virulence, Disease and Defense
Nucleosides and Nucleotides
Cell Wall and Capsule
Dormancy and Sporulation
Regulation and Cell signaling
Nitrogen Metabolism
Sulfur Metabolism
Cell Division and Cell Cycle
Secondary Metabolism
Cofactors, Vitamins, Prosthetic Groups, Pigments
Potassium metabolism
Motility and Chemotaxis
Phages, Prophages, Transposable elements, Plasmids
RNA Metabolism
Amino Acids and Derivatives
Photosynthesis
Stress Response
Protein Metabolism
Membrane Transport
Phosphorus Metabolism
Miscellaneous
Fatty Acids, Lipids, and Isoprenoids
Respiration
DNA Metabolism
Metabolism of Aromatic Compounds
Clustering-based subsystems

D

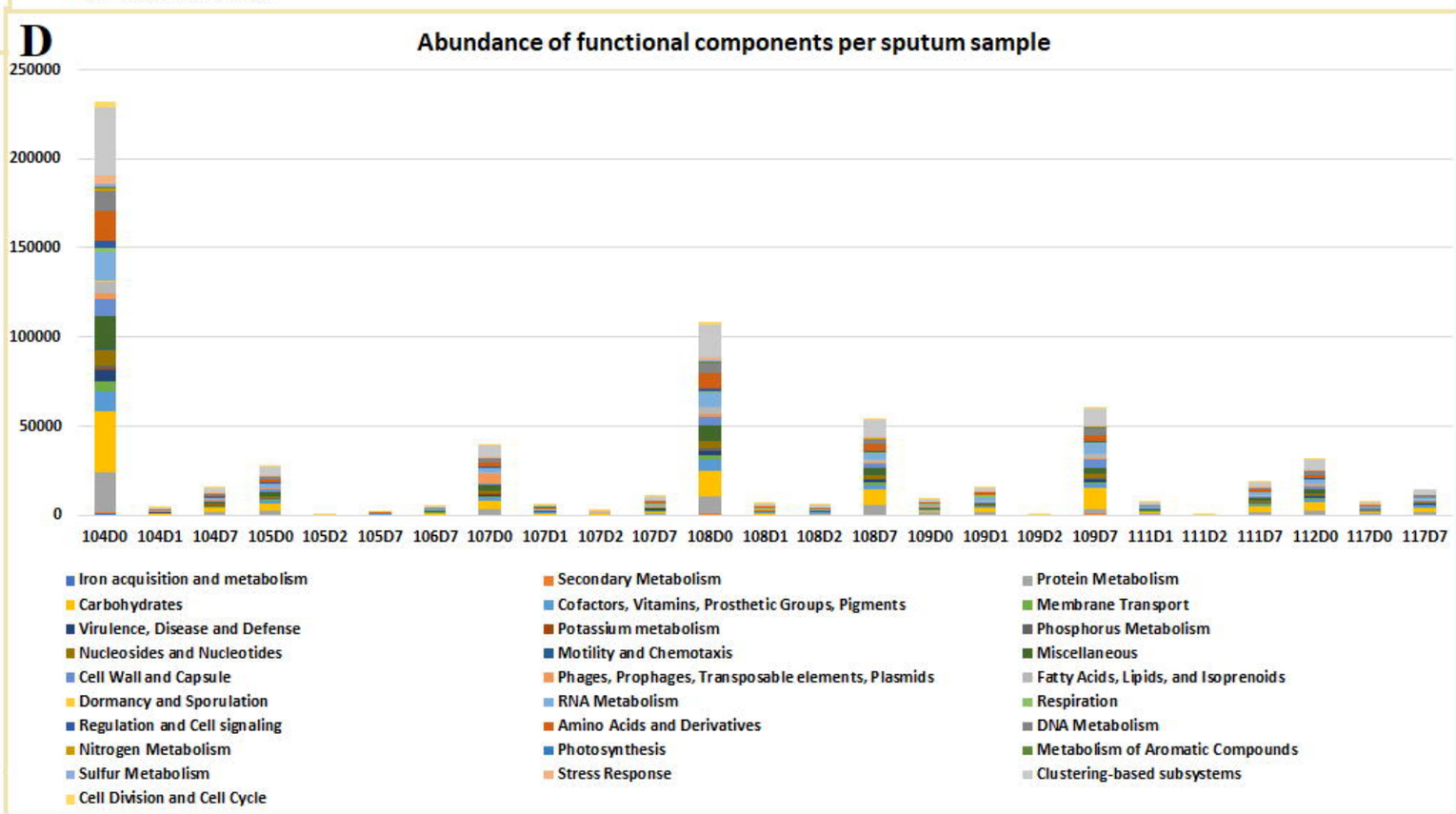
Abundance of functional components per sputum sample
104D0 104D1 104D7 105D0 105D2 105D7 106D7 107D0 107D1 107D2 107D7 108D0 108D1 108D2 108D7 109D0 109D1 109D2 109D7 111D1 111D2 111D7 112D0 117D0 117D7
Iron acquisition and metabolism
Carbohydrates
Virulence, Disease and Defense
Nucleosides and Nucleotides
Cell Wall and Capsule
Dormancy and Sporulation
Regulation and Cell signaling
Nitrogen Metabolism
Sulfur Metabolism
Cell Division and Cell Cycle
Secondary Metabolism
Cofactors, Vitamins, Prosthetic Groups, Pigments
Potassium metabolism
Motility and Chemotaxis
Phages, Prophages, Transposable elements, Plasmids
RNA Metabolism
Amino Acids and Derivatives
Photosynthesis
Stress Response
Protein Metabolism
Membrane Transport
Phosphorus Metabolism
Miscellaneous
Fatty Acids, Lipids, and Isoprenoids
Respiration
DNA Metabolism
Metabolism of Aromatic Compounds
Clustering-based subsystems

E

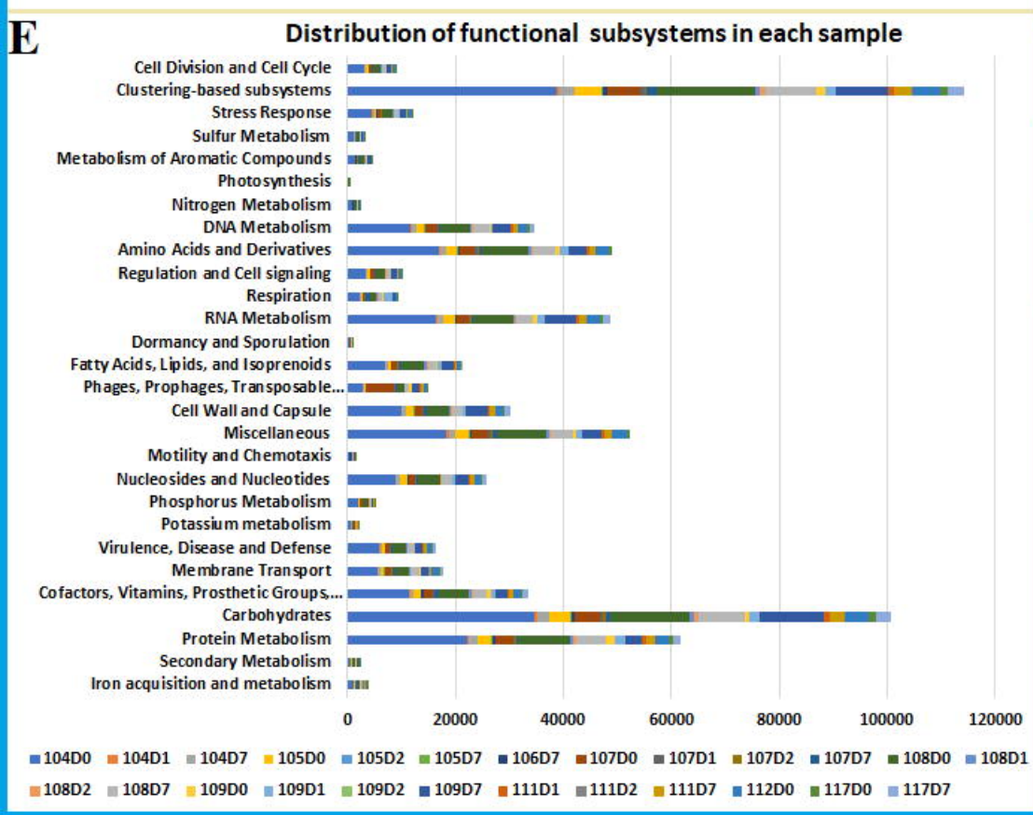
Distribution of functional subsystems in each sample
Cell Division and Cell Cycle
Clustering-based subsystems
Stress Response
Sulfur Metabolism
Metabolism of Aromatic Compounds
Photosynthesis
Nitrogen Metabolism
DNA Metabolism
Amino Acids and Derivatives
Regulation and Cell signaling
Respiration
RNA Metabolism
Dormancy and Sporulation
Fatty Acids, Lipids, and Isoprenoids
Phages, Prophages, Transposable...
Cell Wall and Capsule
Miscellaneous
Motility and Chemotaxis
Nucleosides and Nucleotides
Phosphorus Metabolism
Potassium metabolism
Virulence, Disease and Defense
Membrane Transport
Cofactors, Vitamins, Prosthetic Groups,...
Carbohydrates
Protein Metabolism
Secondary Metabolism
Iron acquisition and metabolism
104D0 104D1 104D7 105D0 105D2 105D7 106D7 107D0 107D1 107D2 107D7 108D0 108D1 108D2 108D7 109D0 109D1 109D2 109D7 111D1 111D2 111D7 112D0 117D0 117D7

A

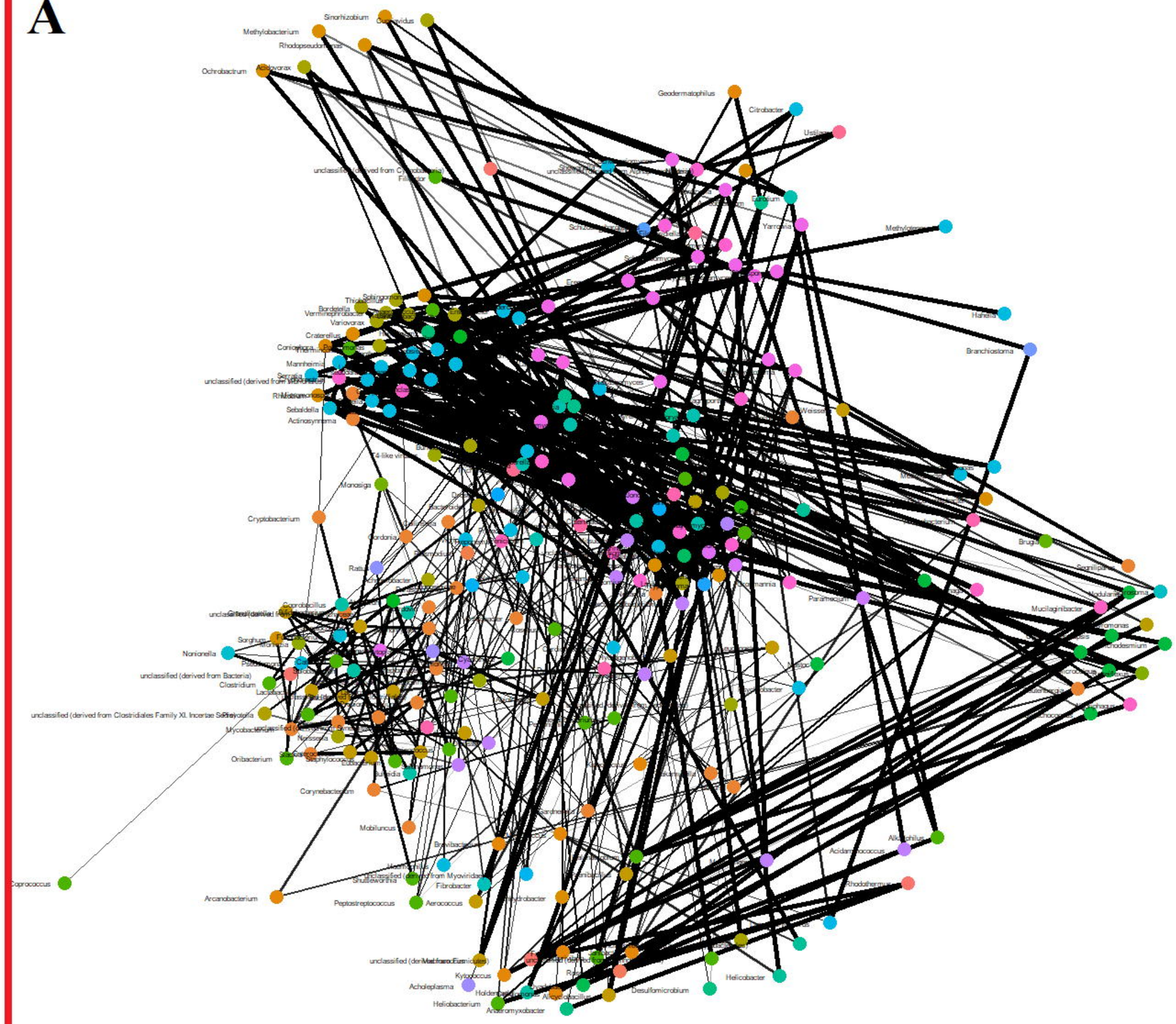

Class

- Alphaproteobacteria
- Aconoidasida
- Actinobacteria
- Actinomycetia
- Agaricomycetes
- Alphaproteobacteria
- Angiosperms
- Aquificae
- Bacilli
- Bacteroidetes
- Bacteroidia
- Betaproteobacteria
- Caudoviricetes
- Cestoda
- Chloroflexi
- Choanoflagellatea
- Chromadorea
- Clostridia
- Conoidasida
- Coriobacteriia
- Cyanophyceae
- Cytophagia
- Dehalococcoidetes
- Delta Proteobacteria
- Deltaproteobacteria
- Dothideomycetes
- Epsilonproteobacteria
- Erysipelotrichia
- Eurotiomycetes
- Fibrobacteria
- Flavobacteriia
- Foraminifera
- Fusobacteriia
- Gammaproteobacteria
- Herviviricetes
- Heunggongvirae
- Holozoa
- incertae sedis
- Insecta
- Kinetoplastea
- Leotiomycetes
- Leptocardii
- Mammalia
- Mollicutes
- Mucorales
- Negativicutes
- Oligohymenophorea
- Onygenales
- Revtraviricetes
- Rhabditophora
- Saccharomycetes
- Saccharomycotina
- Schizosaccharomycetes
- Sordariomycetes
- Sphingobacteriia
- Spirochaetales
- Synergistia
- Thermoleophilia
- Tremellomycetes
- Trichozoa
- Ustilaginomycetes

Distance

- 0.0
- 0.2
- 0.4
- 0.6

B

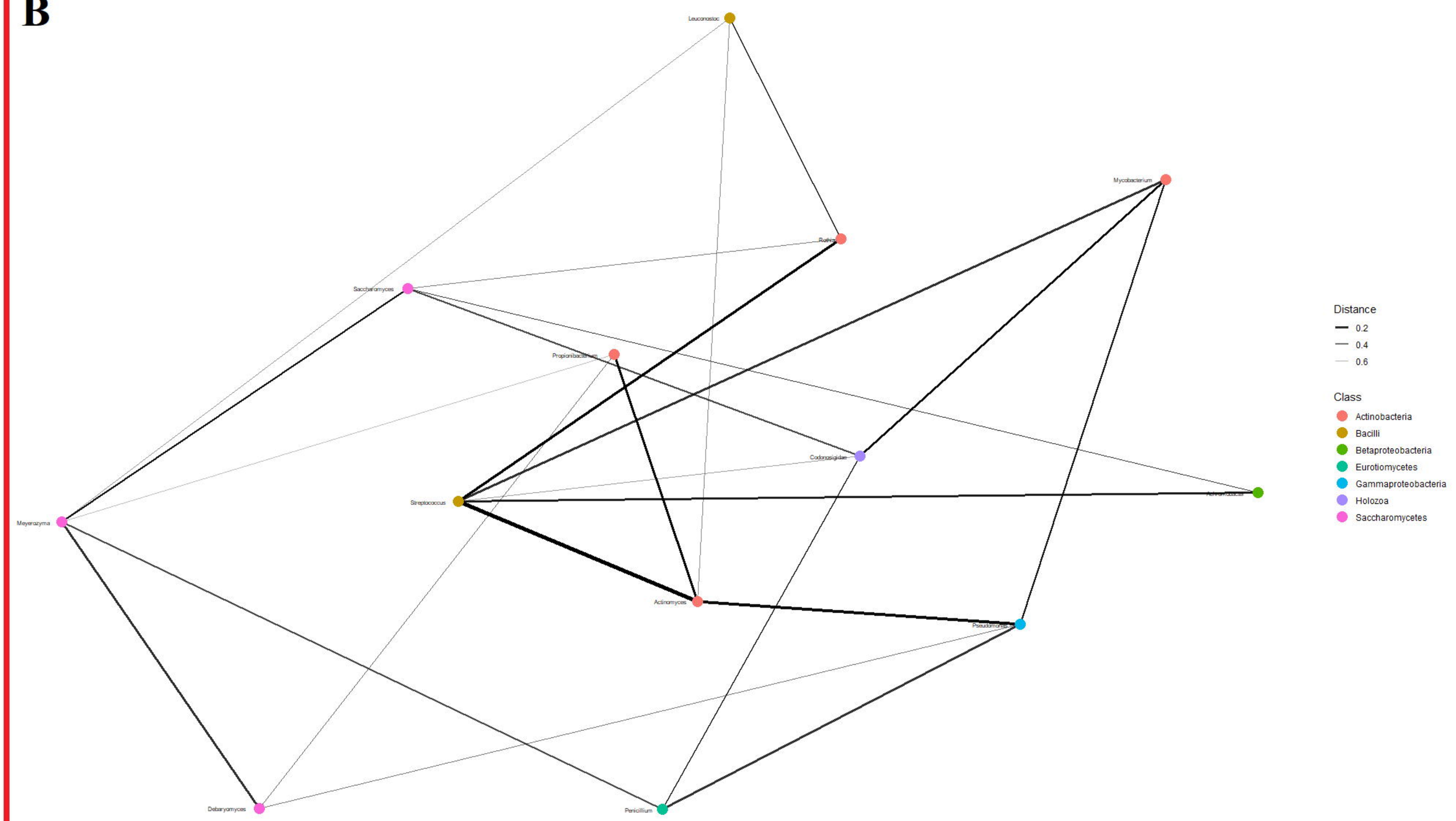

Distance

- 0.2
- 0.4
- 0.6

Class

- Actinobacteria
- Bacilli
- Betaproteobacteria
- Eurotiomycetes
- Gammaproteobacteria
- Holozoa
- Saccharomycetes

C

OTUs

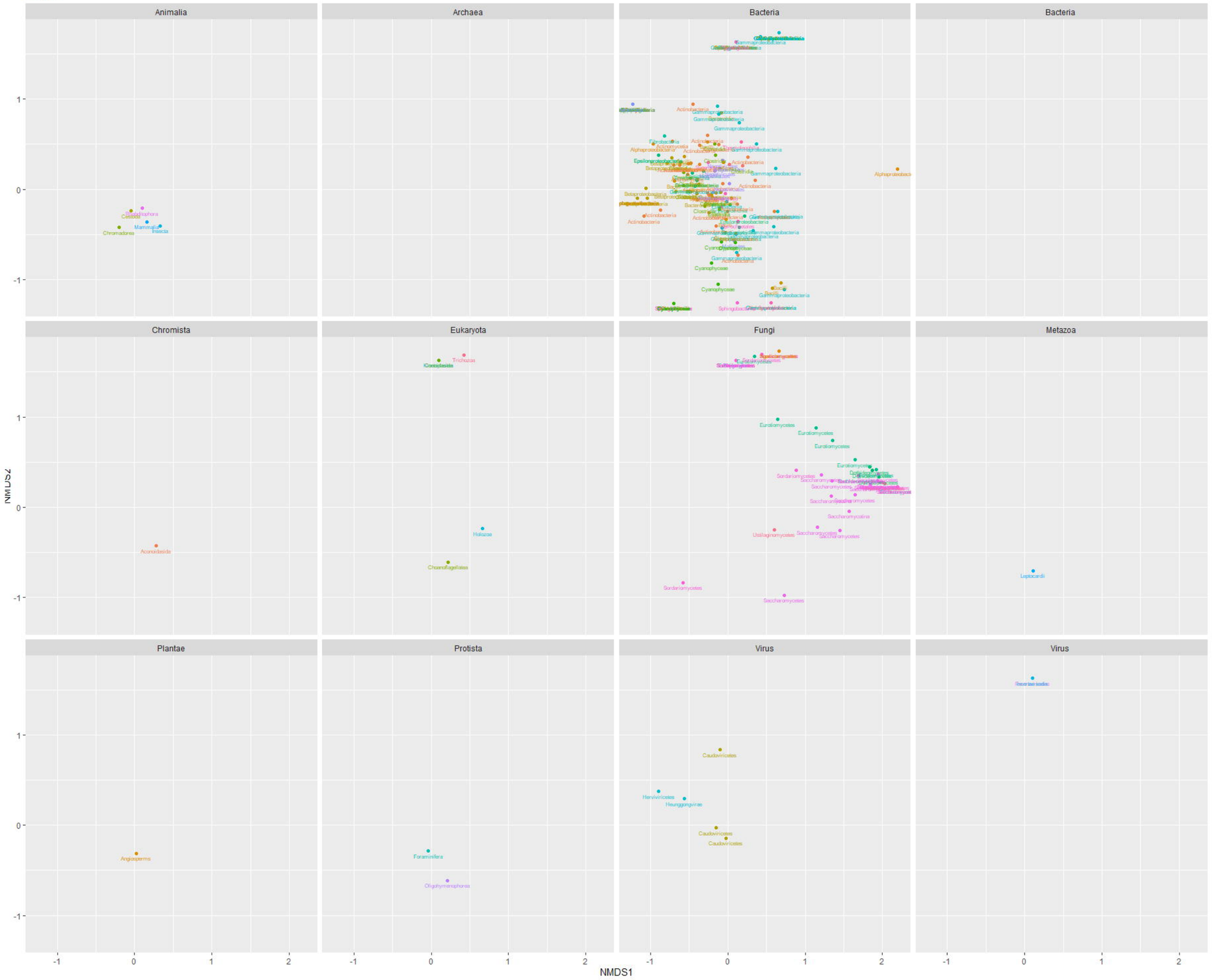
Animalia
Archaea
Bacteria
Bacteria
Chromista
Eukaryota
Fungi
Metazoa
Plantae
Protista
Virus
Virus
NMDS1
NMDS2


Class
Alphaproteobacteria
Aconoidasida
Actinobacteria
Actinomycetia
Agaricomycetes
Alphaproteobacteria
Angiosperms
Aquificae
Archaeoglobi
Bacilli
Bacteroidetes
Bacteroidia
Betaproteobacteria
Caudoviricetes
Cestoda
Chlorobi
Chloroflexi
Choanoflagellatea
Chromadorea
Clostridia
Conoidasida
Coriobacteriia
Cyanophyceae
Cytophagia
Dehalococcoidetes
Deinococci
Delta Proteobacteria
Deltaproteobacteria
Dothideomycetes
Epsilonproteobacteria
Erysipelotrichia
Eurotiomycetes
Exobasidiomycetes
Fibrobacteria
Flavobacteriia
Foraminifera
Fusobacteriia
Gammaproteobacteria
Herviviricetes
Heunggongvirae
Holozoa
incertae sedis
Insecta
Kinetoplastea
Ktedonobacteria
Leotiomycetes
Leptocardii
Mammalia
Methanococci
Methanomicrobia
Methylacidiphilae
Mollicutes
Mucorales
Negativicutes
Nitrospira
Oligohymenophorea
Onygenales
Opitutae
Planctomycetia
Revtraviricetes
Rhabditophora
Saccharomycetes
Saccharomycotina
Schizosaccharomycetes
Sordariomycetes
Sphingobacteriia
Spirochaetales
Spirochaetia
Synergistia
Thermodesulfovibrionia
Thermoleophilia
Tissierellia
Tremellomycetes
Trichozoa
Ustilaginomycetes

D

OTUs


Animalia
Archaea
Bacteria
Bacteria
Chromista
Eukaryota
Fungi
Metazoa
Plantae
Protista
Virus
Virus
NMDS1
NMDS2


Class
Alphaproteobacteria
Aconoidasida
Actinobacteria
Actinomycetia
Agaricomycetes
Alphaproteobacteria
Angiosperms
Aquificae
Archaeoglobi
Bacilli
Bacteroidetes
Bacteroidia
Betaproteobacteria
Caudoviricetes
Cestoda
Chlorobi
Chloroflexi
Choanoflagellatea
Chromadorea
Clostridia
Conoidasida
Coriobacteriia
Cyanophyceae
Cytophagia
Dehalococcoidetes
Deinococci
Delta Proteobacteria
Deltaproteobacteria
Dothideomycetes
Epsilonproteobacteria
Erysipelotrichia
Eurotiomycetes
Exobasidiomycetes
Fibrobacteria
Flavobacteriia
Foraminifera
Fusobacteriia
Gammaproteobacteria
Herviviricetes
Heunggongvirae
Holozoa
incertae sedis
Insecta
Kinetoplastea
Ktedonobacteria
Leotiomycetes
Leptocardii
Mammalia
Methanococci
Methanomicrobia
Methylacidiphilae
Mollicutes
Mucorales
Negativicutes
Nitrospira
Oligohymenophorea
Onygenales
Opitutae
Planctomycetia
Revtraviricetes
Rhabditophora
Saccharomycetes
Saccharomycotina
Schizosaccharomycetes
Sordariomycetes
Sphingobacteriia
Spirochaetales
Spirochaetia
Synergistia
Thermodesulfovibrionia
Thermoleophilia
Tissierellia
Tremellomycetes
Trichozoa
Ustilaginomycetes